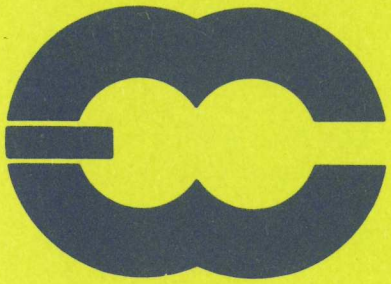

European Centre for Medium Range Weather Forecasts

A Study of the Effect of an Interactive Radiation Scheme on a Medium Range Forecast

Internal Report 20
Research Dept.

December 1978

Centre Européen pour les Prévisions Météorologiques à Moyen Terme

Europäisches Zentrum für mittelfristige Wettervorhersage

A study of the effect of an interactive radiation scheme on a medium range forecast

By

A. Hollingsworth and K. Arpe

European Centre for Medium Range Weather Forecasts
Bracknell, Berks.

Internal Report No.20

Research Department December 1978

N O T E :

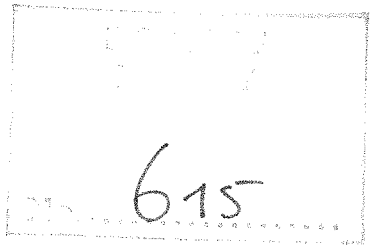

1. Introduction

The problem of medium range weather forecasting is rather different from the problem of short range weather forecasting. The time scale for the more subtle effects of energy sources and sinks in the atmosphere is longer than the two to three days for which short range forecasts are made. Hence in these forecasts fairly crude representations of the main energy sources and sinks in the atmosphere are often adequate. For medium range forecasts the interactions of the inertial effects and the energy sources and sinks are more important.

The main energy sources of the atmosphere are radiation and latent heat release. The radiation field is profoundly affected by the distribution and properties of clouds. Clouds in turn owe their existence to the condensation process in which large amounts of latent heat are released to the atmosphere, often at large distances from the places where the water vapour was introduced to the atmosphere.

For these reasons much effort will be devoted to the study of the questions of cloud prediction, the modification of the radiative heating field by clouds and the mutual effects of this process and the motion field which produces the clouds.

In this study we took the 9 level N48 GFDL model used in ARPE, BENGTSSON, HOLLINGSWORTH and JANJIĆ (1976) (later referred to as ABH&J), modified the treatment of clouds in the model in a simple fashion and analysed the consequences for a ten-day forecast.

The main findings are that

1) omission of a parameterization of cumulus cloud leads to an underestimate of cloudiness in the tropics. This leads to greater surface heating and long wave radiative loss in the free atmosphere in these regions. As a result a stronger vertical lapse rate was created which caused more convective precipitation.

2) There is a cooling of the atmosphere in polar regions of 2 K over the 10-day period. This is accompanied by a rise in surface pressure of some 10 - 15 mb compared with the control run with GFDL physics. This leads to errors in the zonally averaged geopotential near the pole.

3) The parameterization gave good fields of medium-level cloudiness when compared to observations in mid-latitude. The parameterization produced very similar cloud distributions for all three levels which is not always true in the real atmosphere.

4) There were some slight gains in forecast skill during the first seven days when the interactive scheme was used, but after seven days appreciable differences became obvious which in most cases gave worse skill for the interactive scheme run.

5) The fact that the differences between the runs were rather marginal is thought to be due to the fact that the treatment of cloud and humidity in the radiation calculation in both models is not free of climatological specifications.

In Section 2 we describe the changes to the cloud representation and in Section 3 we describe in detail the comparisons of our forecast with a control experiment.

2. Cloud parameterization

The GFDL model we used has been described in an earlier report (ABH&J, 1976). In this model, clouds are specified by climatological averages at three levels of the model. The quantities specified as functions of latitude only are the height of the cloud, the fractional cloud cover, the cloud reflectivity and the cloud absorptivity. The reflectivities were 0.21, 0.48, 0.69 for high, medium and low clouds respectively while the corresponding absorptivities were .005, .02, .035, for the whole globe. The cloud amounts and cloud heights are specified as functions of latitude only and are shown in figs. 3.1.4 and 2.1.1 respectively.

In our run we altered the specification of clouds by making the occurrence depend on the relative humidity and the sign of the vertical velocity, averaged over the previous six hours. The cloud is assumed to have the same optical properties and height as in the control run. Cloud can only occur if the time averaged vertical velocity > 1cm/sec. The values of the constants used in the regressions on humidity were taken from Hunt (personal communication). The values used were as follows, r being the relative humidity and c the cloud amount :

Low cloud	$c = 0$	$r < .5$
	$= (r-.5)/.4$	$.5 \leq r \leq .9$
	$= 1$	$.9 \leq r$
Medium cloud	$c = 0$	$r < .55$
	$= (r-.55)/.45$	$.55 \leq r$
High cloud	$c = 0$	$r < .55$
	$= .7\ (r-.55)/.45$	$.55 \geq r$

Some preliminary experiments indicated that the radiative field was insensitive to a choice of 1 cm/sec. or 0.5 cm/sec. as the cut-off point on the vertical velocity.

This scheme was implemented in our run at day one, because we needed a time history of vertical velocity.

3. Results

When comparing the forecast with a radiation interaction scheme we shall refer to it in the figures as "RAD-run" and the control run using climate cloud data we refer to as "N48-run". Only brief comparisons between the forecasts and the verifying analyses will be given because that has been done already by ABH&J(1976) and only differences in the forecasts will be noted. The comparison was mainly made by means of programs already used by ABH&J and therefore there is usually a restriction in the area for verification to the troposphere north of 20^{o}N.

3.1 Cloud distribution

To show the quality of the cloud parameterization, fig. 3.1.1 to fig. 3.1.3 gives the distribution of the clouds for day 1. For comparison the operational NMC analyses of clouds are shown in the lower map. On these maps we also give frontal zones which were drawn by hand using forecast surface pressure and 850 mb temperature maps. They agree quite well with those in the routine analysis of the German Weather Service. The cloud distribution is smoothed by zonal Fourier series with maximum wave number 20. This representation hardly changes any of the features of the distribution.

The medium clouds in fig. 3.1.2 show the best agreement between predicted and observed clouds. These clouds are mostly connected with frontal activities. All cloudy areas in our experiment have a corresponding cloudy area in the analyses but the analyses show mostly higher values of cloud amount as well as areas of cloud which are not predicted. This is especially true for regions south of 30°N where there are some doubts if the analysis is right. We do not expect such cloudiness over the deserts of North Africa or Arabia as found in the analysis.

In our experiment all cloud layers show very similar distributions with less cloudiness for the high clouds (fig. 3.1.3) and more cloudiness for the low clouds (fig. 3.1.1). This does not always agree with analyses and therefore the comparison with analyses is not as favourable for low and high clouds as it is for medium clouds.

The differences in intensity with height can best be seen in fig. 3.1.4 which shows zonal means of cloud cover in per cent for the three layers. Results of our parameterization on day 2 and for a 10-day mean can be compared with the climatological values used by GFDL and with analyses by NMC.

The main feature is the excessively low cloudiness at the high level for the whole globe and at the low level for tropical and subtropical regions. The parameterization of the mid-level clouds seems to work quite well in our run. This is probably due to the fact that these clouds are mainly generated by vertical motion of the scales of cyclones, which will be best represented by our scheme.

The differences in tropical and subtropical regions of low level clouds are probably connected with the non-parameterization of cumulus clouds which would probably give the main contribution. On the other hand we do not know how reliable the climatological data are. The analyses obviously give wrong values south of 30°N. High level clouds are underpredicted, while the GFDL values seem to be too high compared with analyses. In fig. 3.1.5 we can see the influence of these different cloud distributions on the non-adiabatic heating. We show the 10-day mean of the latitudinal variation of different energy sources. As can be expected from fig. 3.1.4 the influence is greatest in tropical and subtropical regions, where less cloud means stronger radiative cooling aloft, stronger surface heating, and stronger heating due to rainfall. At 7.5°N and 7.5°S we find some sudden changes in radiative heating which are probably due to sudden changes in cloud heights, which were taken from GFDL in both runs. Taking a mean over the globe for all 10 days the reduced cloudiness gives 0.04 K/day more cooling by radiation, 0.05 K/day more heating by condensation, and 0.01 K/day more heating by sensible heat flux. All combined give an extra heating imbalance of 0.02 K/day. This imbalance is reflected in the global mean temperature which increases from 251.56 K at the beginning to 251.81 K in the case of climatological cloud distribution and to 252.01 K in the case with our cloud parameterization. The difference of 0.2 K at day 10 agrees well with the extra heating of 0.02 K/day.

3.2 Comparison of height fields between both forecasts

To give a survey how both forecast height fields differ, fig. 3.2.1 shows the RMS differences and fig. 3.2.2 the anomaly correlation coefficients for the height field of

the troposphere north of 20°N. The definitions of RMS differences, correlation coefficients etc. and the reasons why we chose these spectral groups may be found in ABH&J (1976).

To give a guideline, the values of a persistence forecast versus the N48-run and a climatological normal deviation from climatology are included in the figures. Both runs were identical for the first day which is obvious in the scores. The first exceptional day is the third day when we find for a while bigger differences between both forecasts in both verification scores and for all spectral modes. The second exceptional day is the 7th day when discrepancies begin to grow rapidly. This can be seen in both verification scores and all spectral modes. These days will be looked at more carefully later. Figures 3.2.3 and 3.2.4 show the latitudinal and vertical variations of the RMS-differences. The higher values at mid-latitudes and higher levels are probably due to higher variances of the height fields in these regions.

It is worth mentioning that there is a growth of differences from the pole for the zonal mean (up to 170m) which is so strong that it can be seen also in the figure for the total RMS-differences. To understand this problem we will first consider the temperature field. Although overall, the model atmosphere's mean temperature increases in both runs, the temperature at the pole decreases, presumably as a consequence of the reduced amount of cloud in the radiation run. By day 6 the difference in northern latitudes is ~ 1K and by day 10 it is ~ 2K. A uniform difference of 1K through the depth of the atmosphere between the surface and 200 mb would give an r.m.s. height difference of 22 m. The extra cooling near the poles in the radiation run cannot therefore explain the difference in the zonally averaged geopotential. The remaining source of discrepancy is the surface pressure. Fig. 3.2.5 shows the difference in the

zonal mean surface pressure at day 7,8,9,10 between the two runs. In general the pressure in polar regions is higher in the radiation run, up to 21 mb. This would give rise to an r.m.s. difference in height of up to 170 m in the opposite sense to that induced by the temperature change. It is worth noting that the large day-to-day changes in the pressure in polar regions are almost certainly due to large scale gravity waves. Fig. 3.2.6 shows the mean Northern Hemisphere surface pressure as a function of time in both runs. Part of the data was lost between days 6 and 7 for the N48 run. Both runs show an oscillation of ~ .75 mb amplitude initially. At the outset the phase of the oscillation is the same in both runs. Towards the end of the forecast period the oscillations are in antiphase. These oscillations will have largest amplitude near the pole, thus explaining the marked day to day fluctuations in zonally averaged surface pressure differences.

3.3 Synoptic comparison

In this section a comparison of each forecast with the other and with the verifying NMC-analysis will be carried out. The comparisons with the verifying NMC-analyses will be restricted to those points where differences in the forecasts occur. Figures 3.3.1 to 3.3.8 show maps of the 500 mb height field. Each figure contains maps of both forecasts, a map of their discrepancies and a map of the verifying analysis. There are no maps shown before day 3 because the differences are too small.

On day 3 (fig. 3.3.1) there are two centres of differences, i.e. near Hudson Bay and over Eastern Europe, both regions with strong gradients in the zonal direction. These differences can hardly be seen by comparing the individual maps on the right and are probably generated by small differences in the phases of the troughs. In the following

days the differences decrease and the forecasts seem to be almost identical until day 6. Then again near Hudson Bay a north-south flow with strong gradients in the height field gives bigger differences. But this time a phase difference of about 10^{O} can already be seen and in this point the RAD-run seems to agree better with the verifying NMC-analysis. On the next day the whole trough near Greenland (and ridge at $0^{O}E$) differs in phase which gives some advantage for the RAD-run, but both forecasts look much more similar to each other than to the NMC analyses. From day 8 on differences are spread all over the map and no decision can be made which of the forecasts is better or worse. It should be mentioned, however, that the trough over Europe has a wrong tilt in the RAD-run and that the ridge at $0^{O}E$ is much better in the RAD-run.

Synoptic maps of the 1000 mb-level show that the main features of both runs are very similar and the differences do not give indications about an advantage for either of the runs. Therefore in fig. 3.3.9 only the 10th day forecast is taken as an example.

To give a more comprehensible view of the developments of troughs and ridges Hovmöller's trough-ridge diagrams will be shown in figures 3.3.10 to 3.3.12 for two different horizontal scales. The trough and ridge-axes of the verifying NMC-analyses (lower panel) are copied into the upper panels for the forecasts to make comparison easier. For the long waves (fig. 3.3.10) both forecasts show good skill. The trough over North America ($300^{O}E$) after day 6 is forecast a little better by the N48-run. For medium scale waves (wave numbers 4 to 9, fig. 3.3.11) the agreement between forecasts and observation is considerably worse compared to the long waves. Both forecasts look very similar but the RAD-run has a tendency for too strong troughs and ridges near the end of the forecast period.

In fig. 3.3.12 for the medium scale waves at 1000 mb a tendency of forecasting too large amplitudes after day 8 can be found, especially in the RAD-run. This failure is the same as at 500 mb.

In fig. 3.3.13 we find zonal means of temperature for day 6. In the left panel we see four main segments from the mean temperature of the NMC-analysis : 20^{o} - 40^{o}N strong baroclinity (subtropical front). 40^{o} - 65^{o}N low baroclinity (air masses of mid latitude), 65^{o} - 82^{o}N strong baroclinity (polar front) and 82^{o} - 90^{o}N almost isothermal (polar air masses). This structure was forecast very poorly. Although the differences between both forecasts are small, it might be important for future considerations that the RAD-run produced lower temperatures to the north and thereby a slightly stronger gradient.

The panel on the right shows the vertical structure of the atmosphere at two latitudes. Here only the differences between the forecasts and verifying NMC analyses are shown to get a higher resolution. The figure shows that at 20^{o}N the RAD-run atmosphere is warmer and somewhat less stable than the N48-run atmosphere especially in the lower layers. At 60^{o}N both runs have similar temperature structures.

Summing up, we can say that the differences between both forecasts, found in the previous Section on day 3, are of no importance for the quality of either of the forecasts. The discrepancies from day 7 onwards represent two different effects : slightly better forecasts by the RAD-run on day 6 and 7 and a wrong development in the RAD-run after day 8 of too strong medium scale waves.

3.4 Conventional skill scores

To get an objective comparison between both forecasts and the verifying analyses, the same skill scores will be used as already described by ABH&J(1976). It has to be kept in mind that the differences in the radiation scheme were introduced on day 1 so that no differences will be found before that.

As already found several times when comparing models, there are no significantly different RMS-errors (fig. 3.4.1). Only after day 8 are there some advantages of the N48-run. Some superiority of the RAD-run prior to that day confirms the results gained in Section 3.3.

Anomaly correlation coefficients, shown in fig. 3.4.2, give similar conclusions.

3.5 Energetics

For a first overview for kinetic energy, we see in fig. 3.5.1 an energy spectrum for the troposphere , which is a mean from day 7½ to day 10 and a mean between 40^{o}N and 60^{o}N. It is obvious that the forecasts considerably underestimate the kinetic energy for wave numbers 1, 2 and 3, which is in accordance with other experiments. For higher wave numbers, the agreement is good and follows a -3 power law.

The variation with time is shown in fig. 3.5.2 for different groups of wave numbers already familiar to us. The main feature to be stressed is an unrealistic increase of kinetic energy of medium scale waves from day 8 onwards for the RAD-run. This agrees with our finding when looking at trough-ridge diagrams.

In fig. 3.5.3, which shows its latitudinal distribution, we see that this increase during the end of the forecast period in the RAD-run is not only too strong (by 22%) but also concentrated at 45^{o} rather than 40^{o} latitude.

Fig. 3.5.4 gives the latitudinal and vertical distribution of the shortest waves, averaged from day $4\frac{1}{2}$ to day 7. The maximum values at 300 mb are forecast much too weak and this seems to be in contrast to our earlier statement, based on fig. 3.5.1, which said that there was good agreement for higher wave numbers. But wave number 10 which probably gives the main contribution to the group of shorter waves has also in fig. 3.5.1 a difference of a factor 4 between forecast and observation. Another point which should be stressed are some rather high values of kinetic energy in the shortest waves near the pole.

In fig. 3.5.2 we found good agreement in zonal kinetic energy, but this does not remain when more details are taken into account. Fig. 3.5.5 shows the latitudinal and vertical distribution of mean zonal winds during the end of the forecast period. The results of the RAD-forecast are worst. The subtropical jet core is too weak and the polar jet can hardly be seen in the forecasts. This agrees with the results for the zonally averaged temperature, fig. 3.3.13.

The available potential energy (fig. 3.5.6) which represents the temperature variance, again has too high values from day 7 onwards for wave numbers 4 to 9. The zonal available potential energy (second panel from the top) is mostly too strong which is in accordance with results in Section 3.1, where we found extra heating in the RAD-run in the tropics and cooling in polar regions which will cause stronger latitudinal temperature differences.

Latitude pressure cross sections of available potential energy for long scale waves (fig. 3.5.7) show some unrealistically high values near the pole at lower levels in both runs. These are especially strong for the RAD-run. Similar unrealistic values could be found for medium scale waves.

In fig. 3.5.6 we found excessively high values of zonal available potential energy, especially from day 5 to day 8, and after day 7 a strong increase of available potential energy of wave number 4 to 9. In accordance with this, we find, in fig. 3.5.8, a very strong transfer from zonal to eddy available potential energy for medium scale waves. For long waves we find a defect of transfer after day 7 which is in accordance with a decrease of long wave available potential energy.

4. Summary and conclusions

Although the parameterization of the clouds connected with synoptic systems seems to be quite reasonable, the consequence of non-parameterization of convective clouds is a noticeable effect on the heating balance in the tropics. This probably contributes to a marked additional loss of forecast skill in mid-latitudes from day 7 onwards. But it is not clear if this is the only failure, because we also find a growth of differences near the pole which becomes obvious in the zonal means. This is probably due to gravity wave activity. On the other hand, the chosen parameterization of clouds and its radiative interaction gives some minor improvements up to day 8, that is in the period before the failure in the tropics begins to influence mid-latitudes. The discrepancies in the short waves and the zonal mean near the pole are not

readily discernible on the synoptic charts and will be the subject of further study.

In the original model both the humidity and cloud amount were specified climatologically. In this study we have introduced a new degree of freedom by allowing the model's humidity field to influence the radiation field through the cloud amount. The humidity in the radiation calculation is still specified climatologically. It may be that we observed rather small differences between the runs because our treatment of moisture in the radiation calculation is incomplete in this regard. An integration which takes both effects into account, together with convective clouds in the tropics, could well produce a larger effect.

References

Arpe, K., Bengtsson, L., Hollingsworth, A. and Z.Janjić 1976 A case study of a ten day prediction. ECMWF Technical Report.1 105 p.

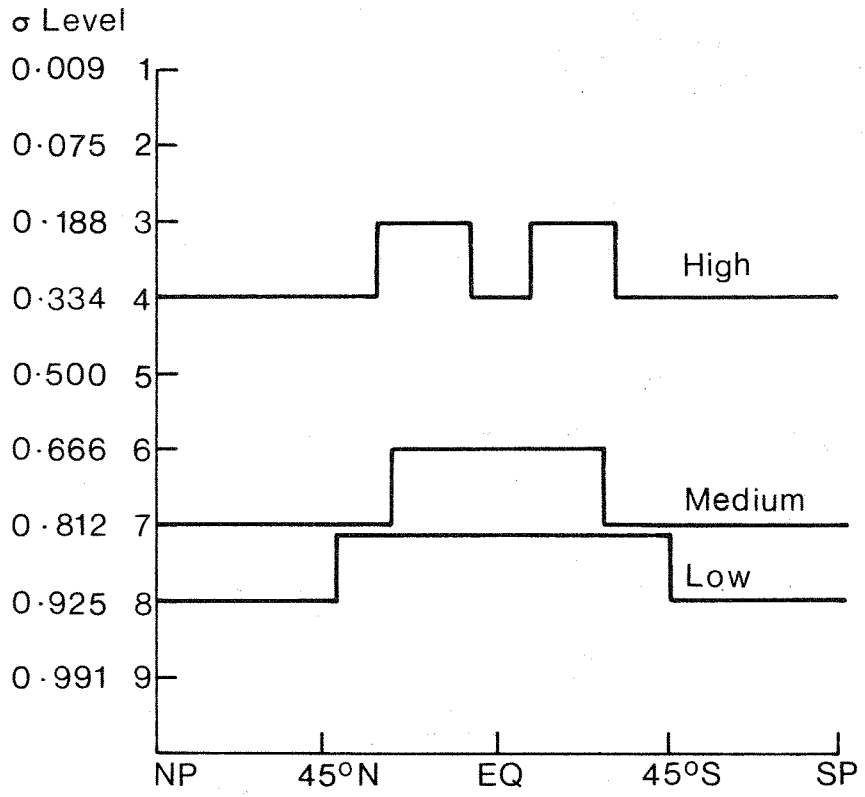

Fig. 2.1.1 Height of high medium and low clouds as functions of latitude.

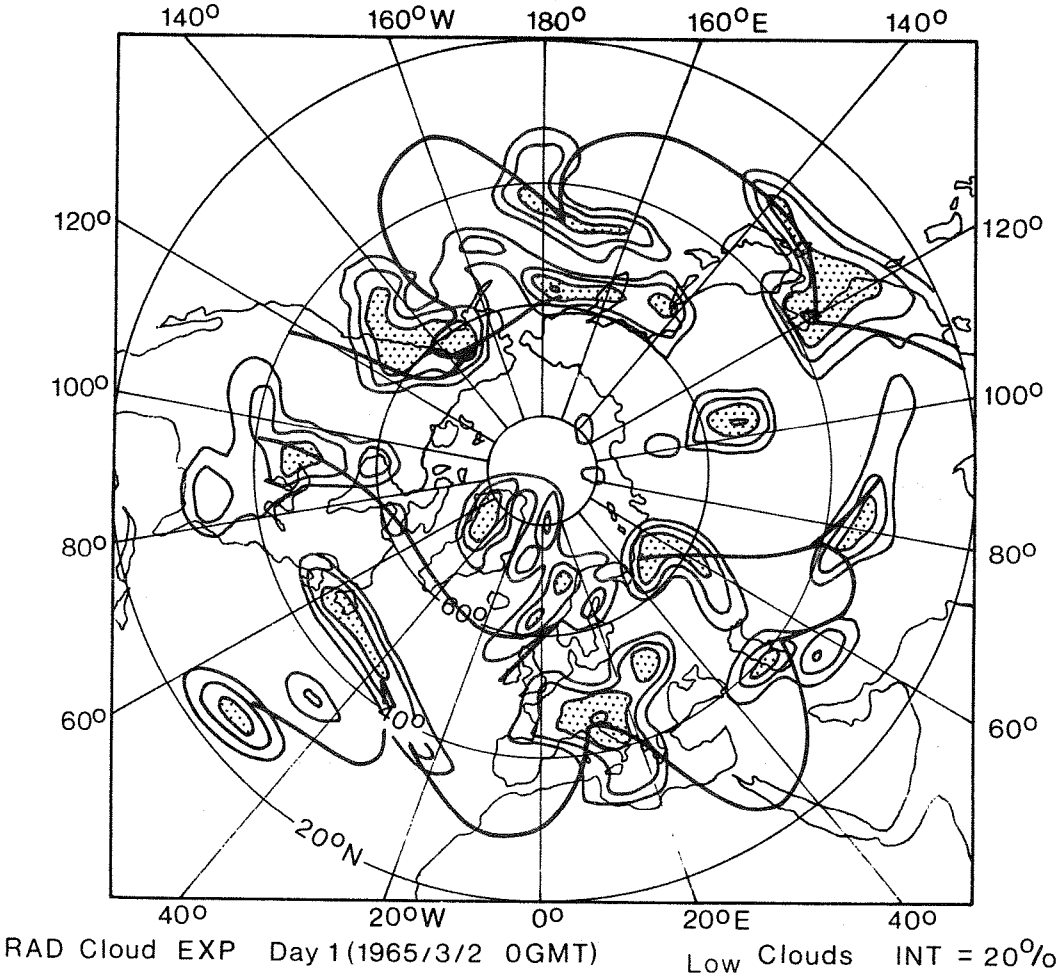

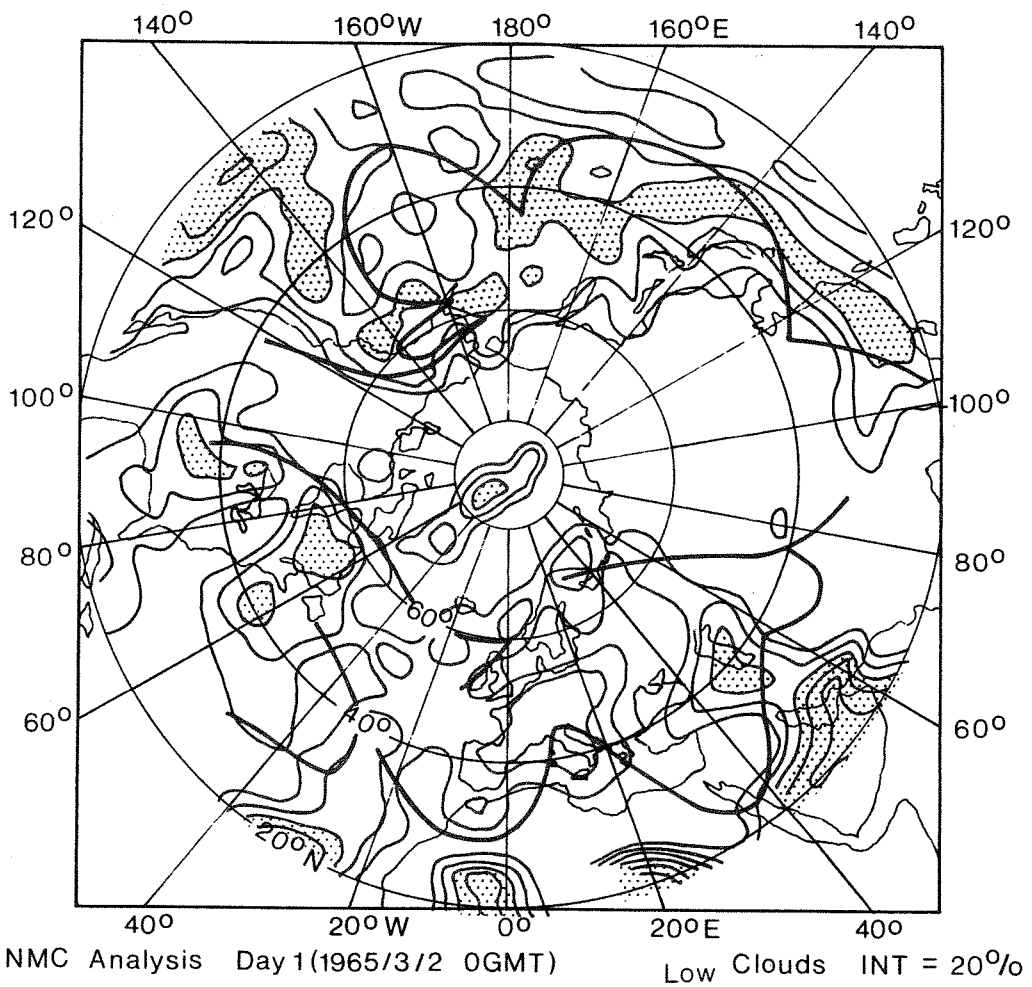

Fig. 3.1.1 Low cloud amount and surface front positions

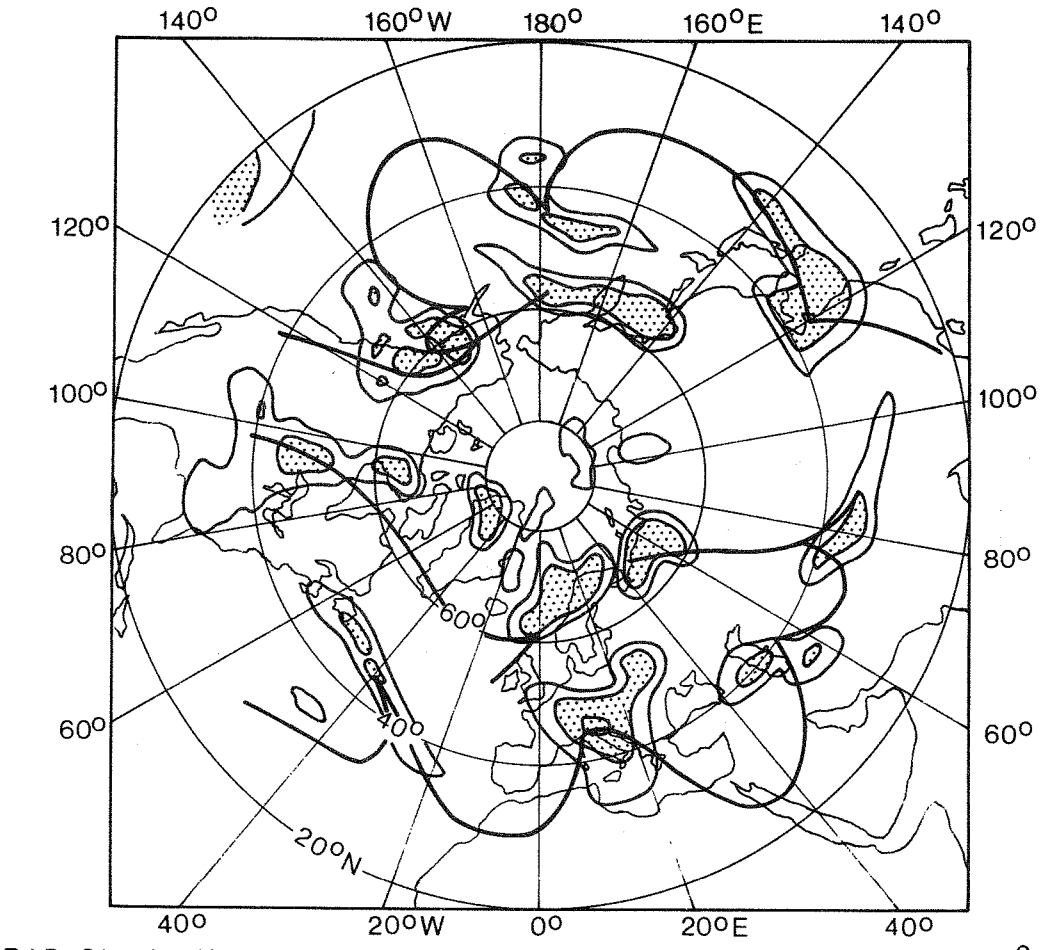

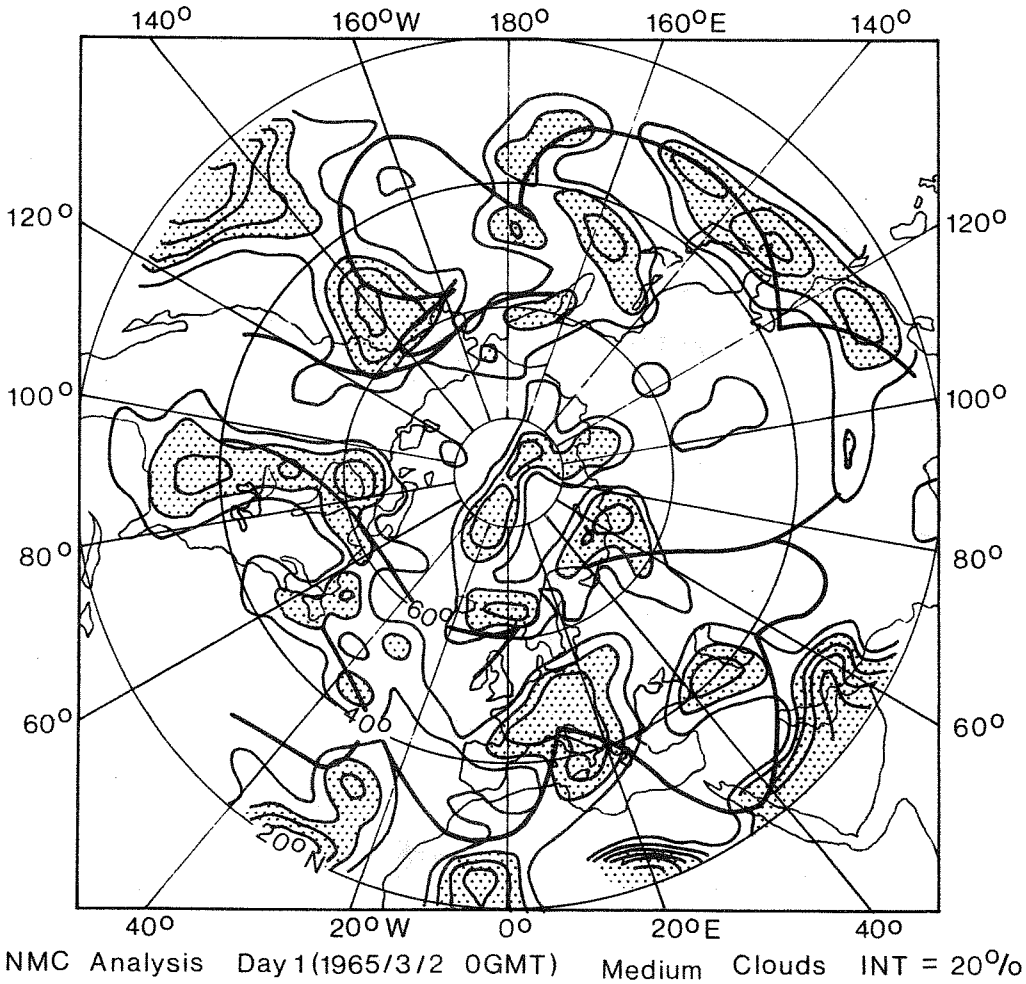

Fig. 3.1.2 Medium cloud amount and surface front positions

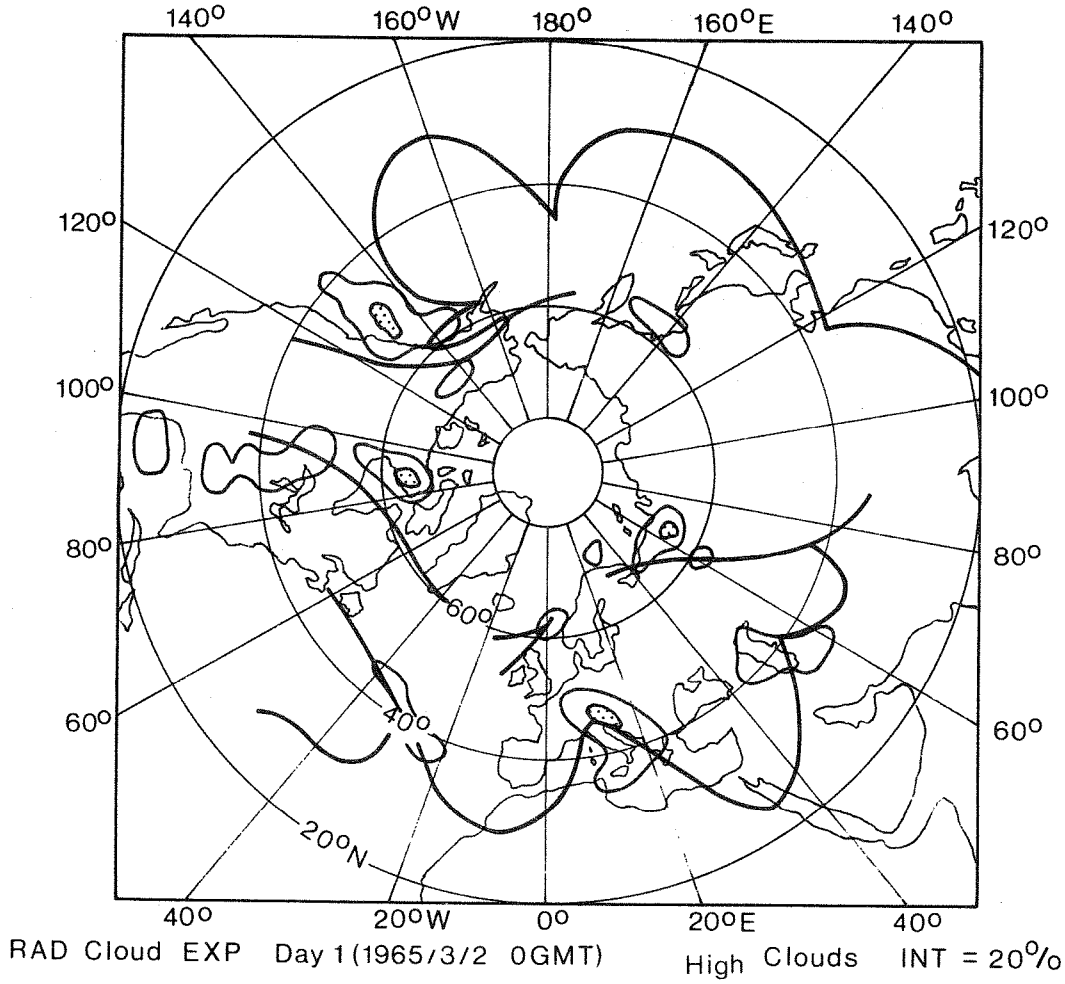

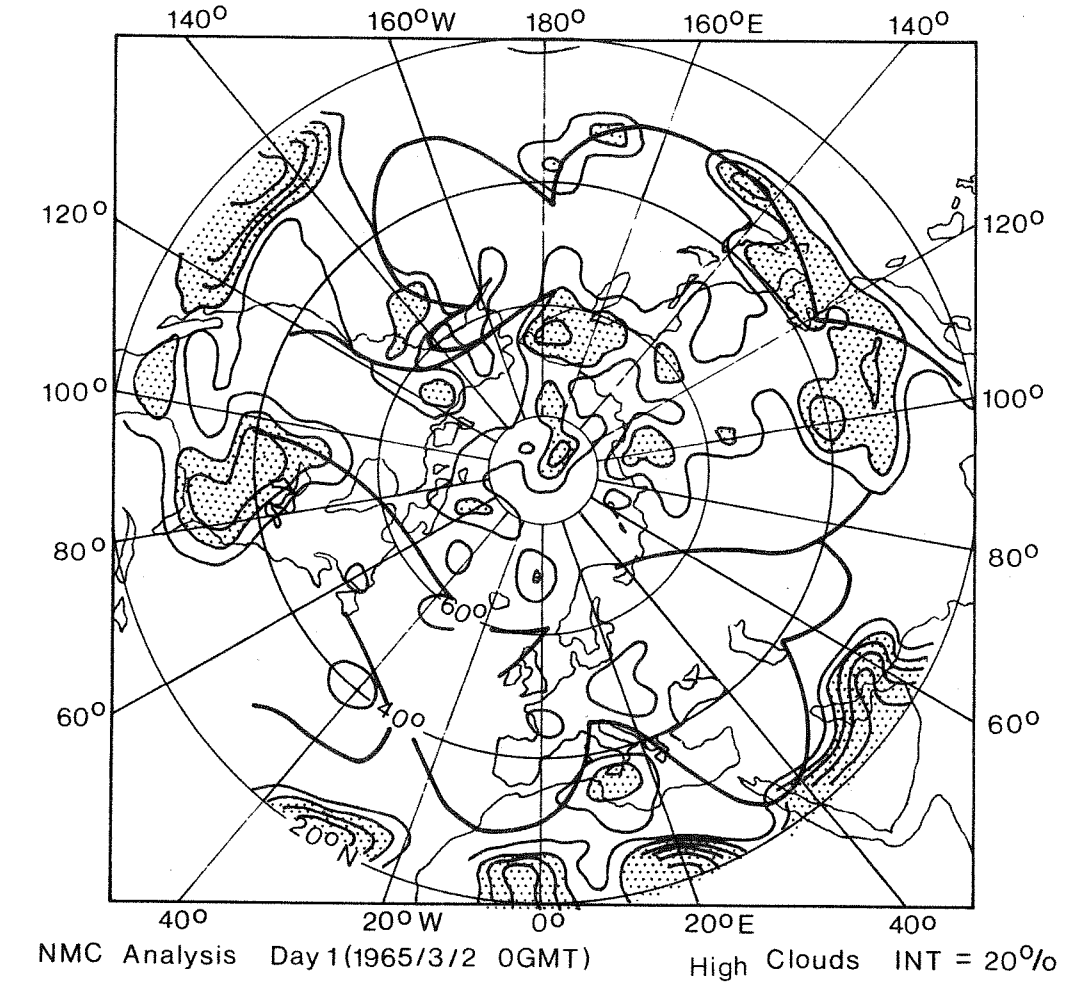

Fig. 3.1.3 High cloud amount and surface front positions

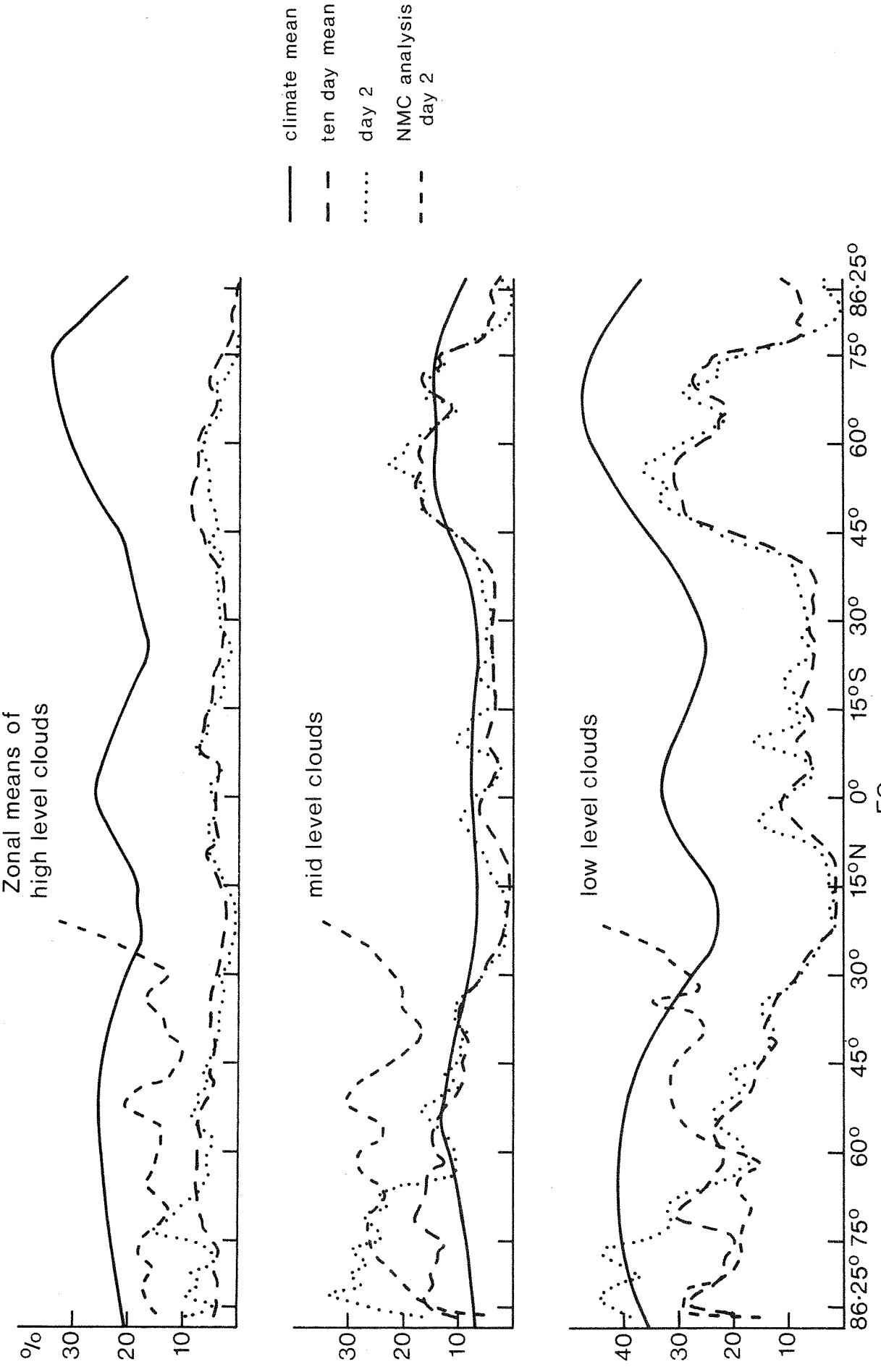

Fig. 3.1.4 Zonal means of high medium and low clouds for the climatic mean, for the ten day mean of the RAD run, for day 2 of the RAD run and for the NMC analysis on day 2.

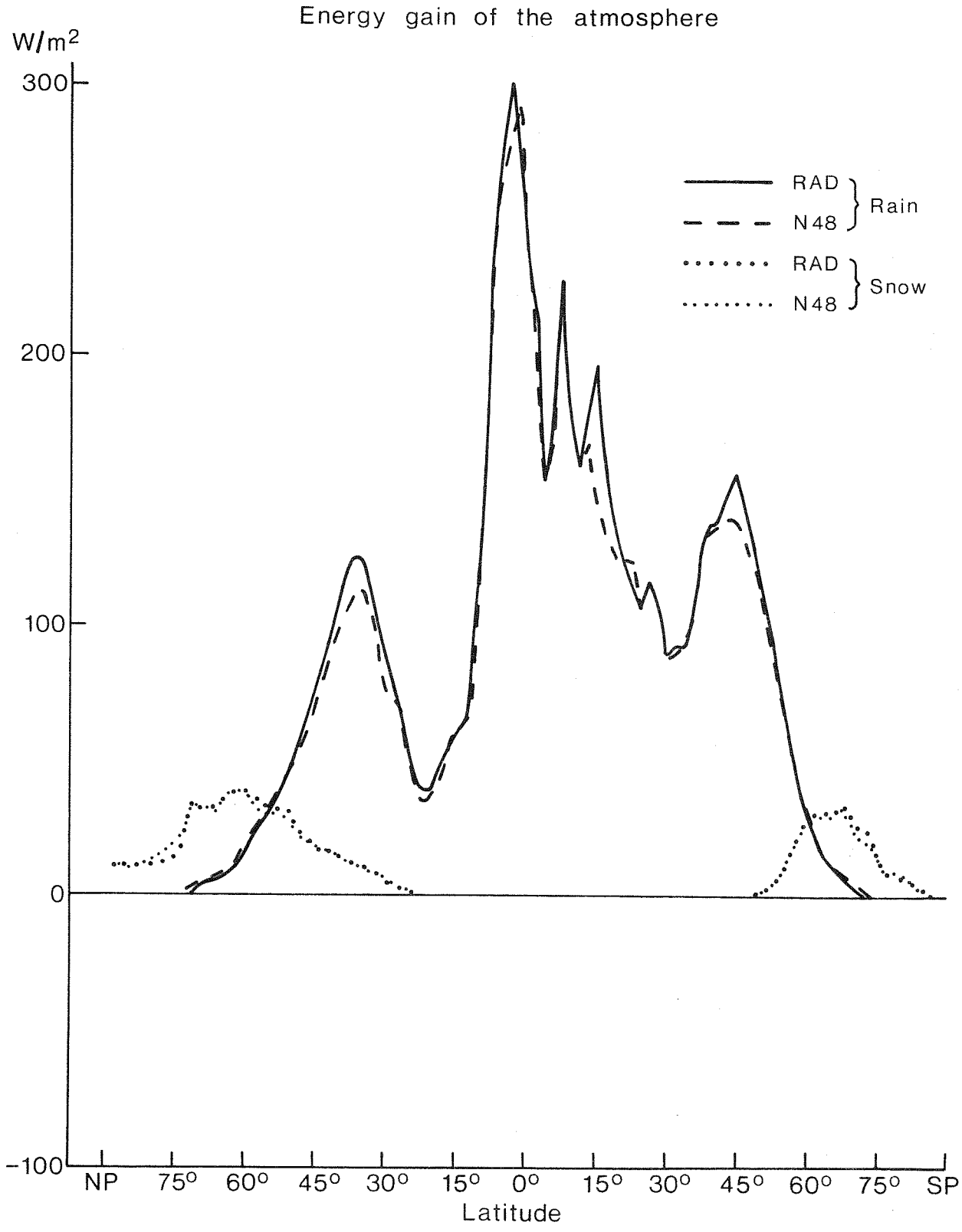

Fig. 3.1.5a. Zonal mean heating rates in the N48 and RAD runs due to rain, snow, surface fluxes and radiation

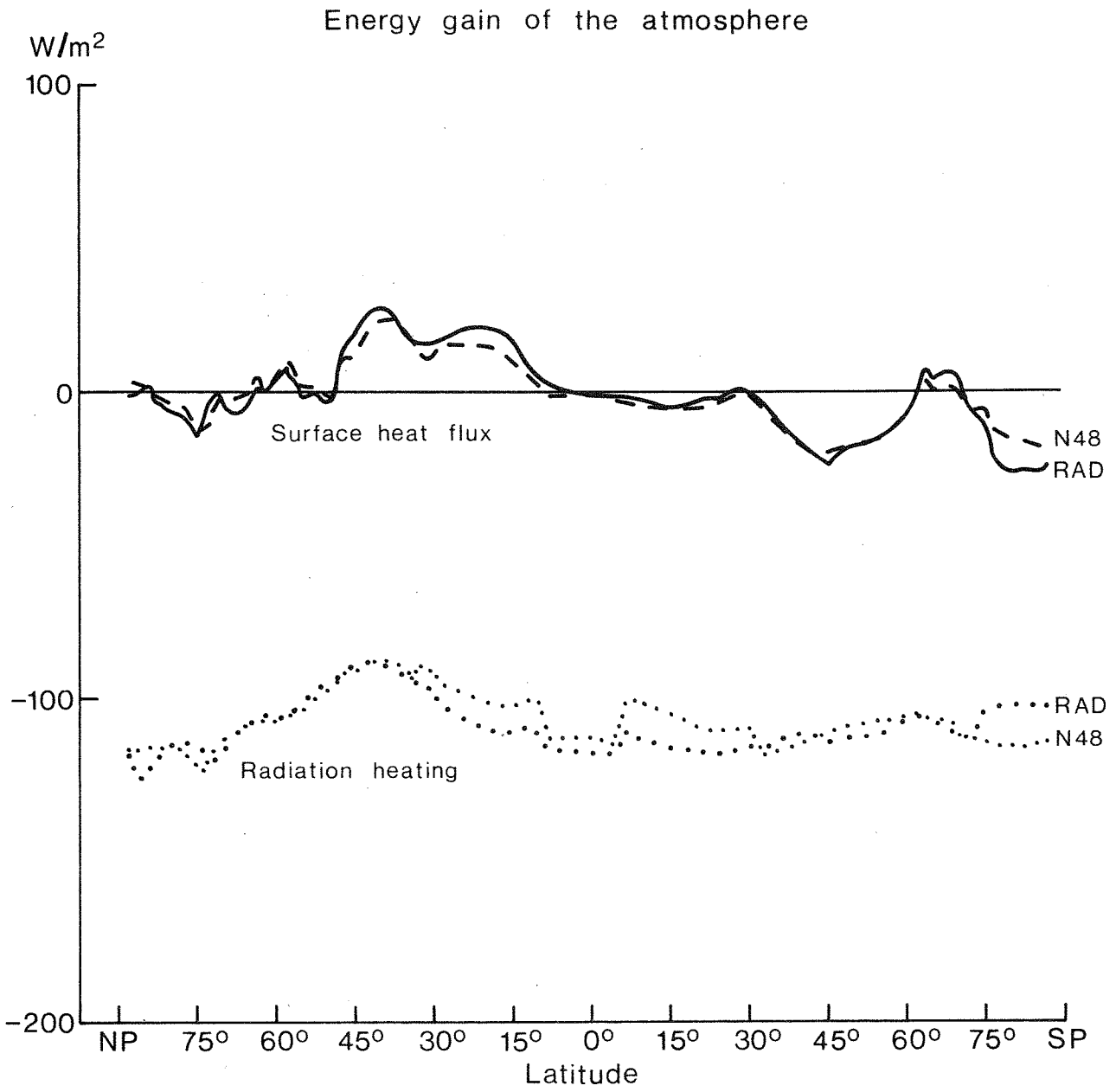

Fig. 3.1.5b. See figure 3.1.5a.

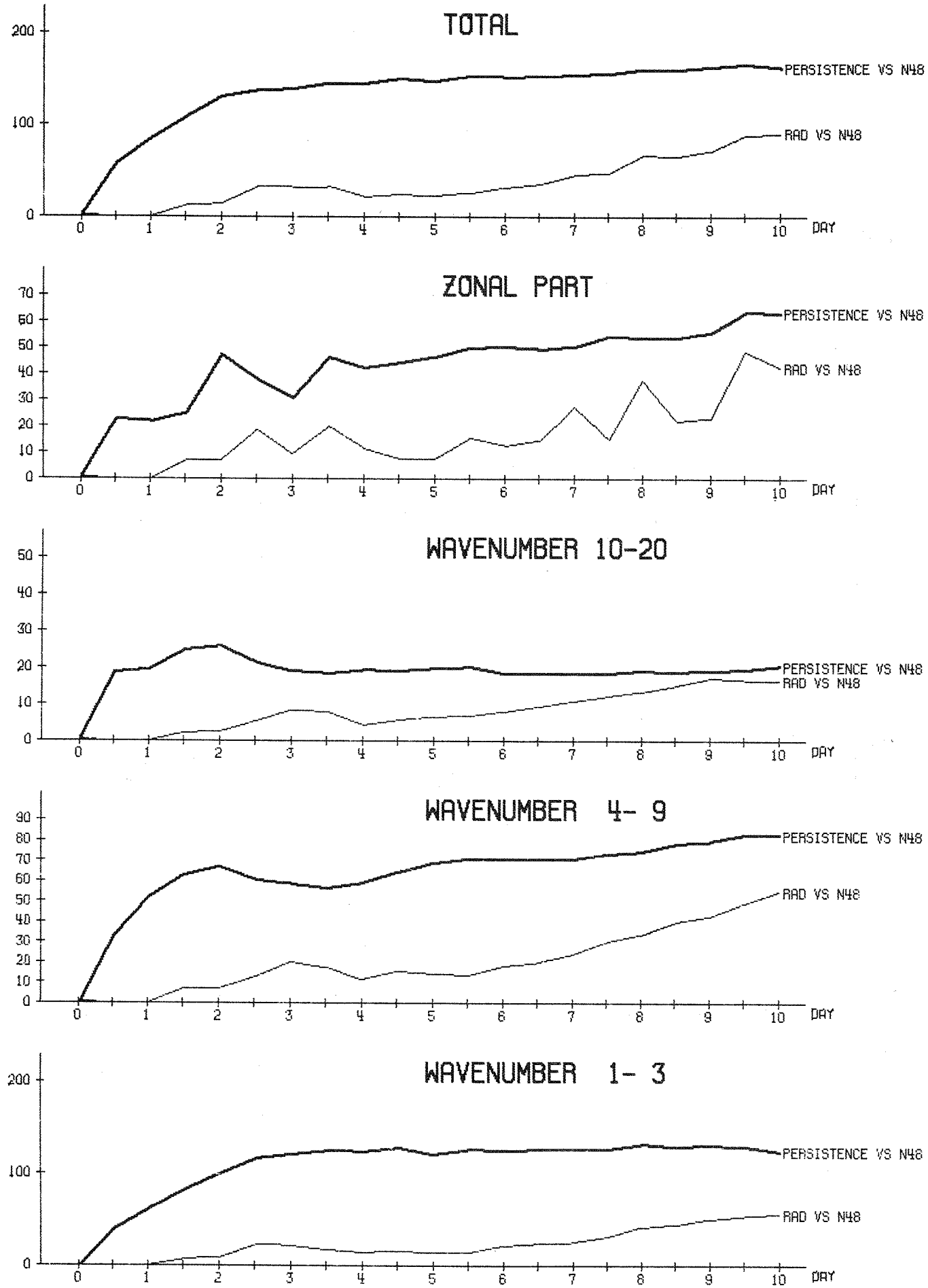

MEAN 1000- 200 MB AND 20.0- 82.5 N RMS HEIGHT DIFFERENCES (M)

Fig. 3.2.1

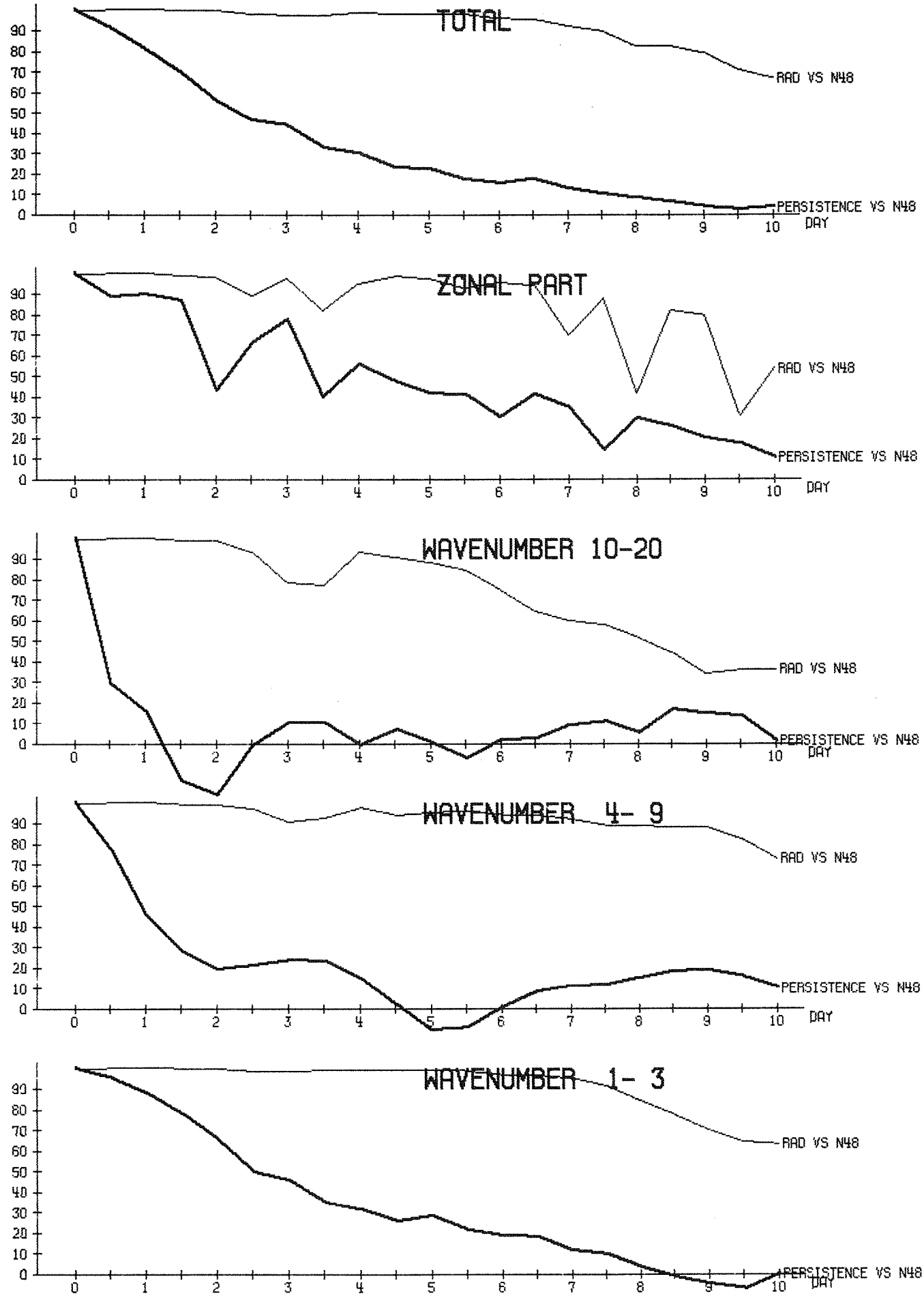

CORRELATION OF HEIGHT % MEAN 1000- 200 MB AND 20.0- 82.5 N

Fig. 3.2.2

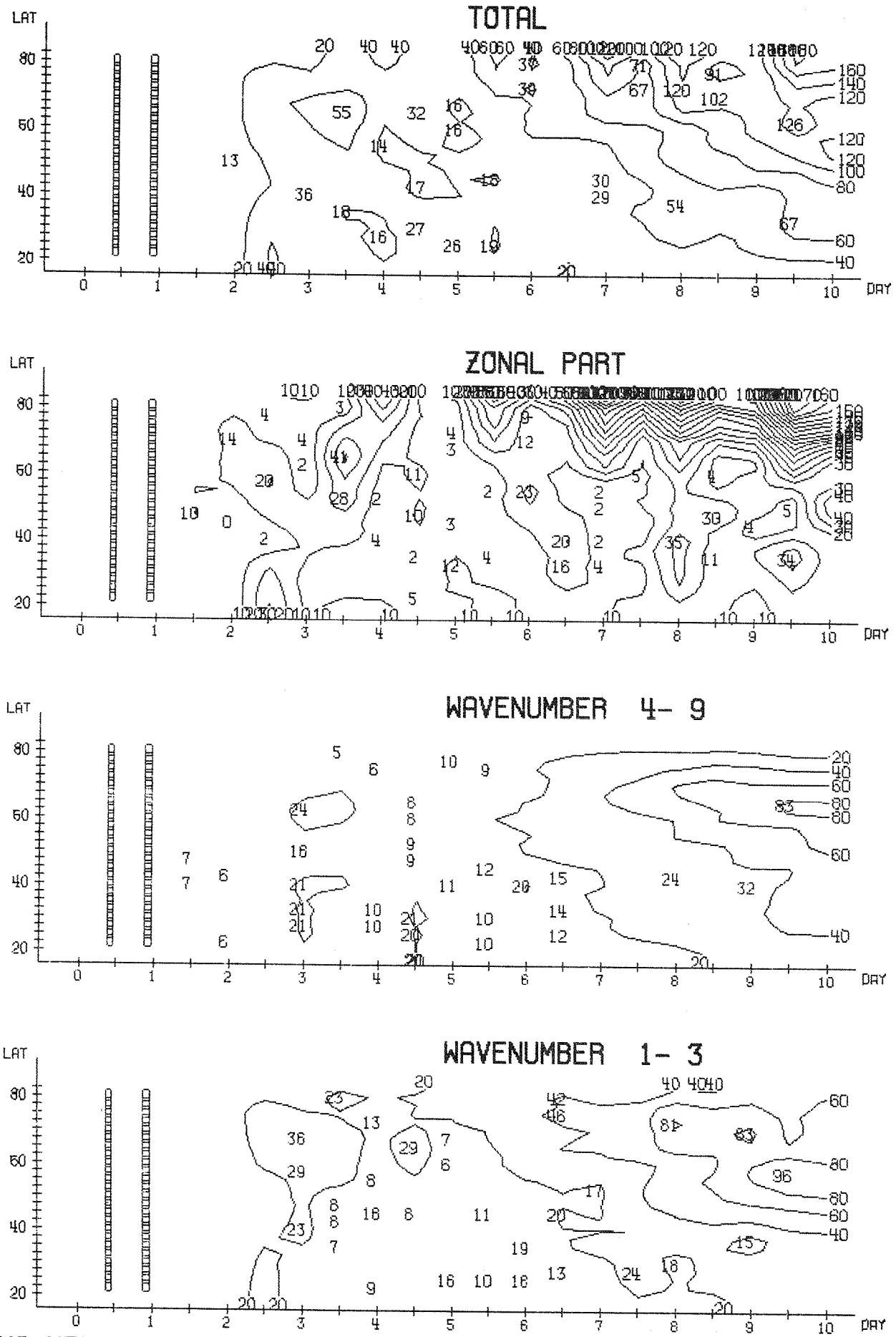

RMS HEIGHT DIFFERENCES (M) MEAN BETWEEN 1000 TO 200 MB
RAD VS N48

Fig. 3.2.3

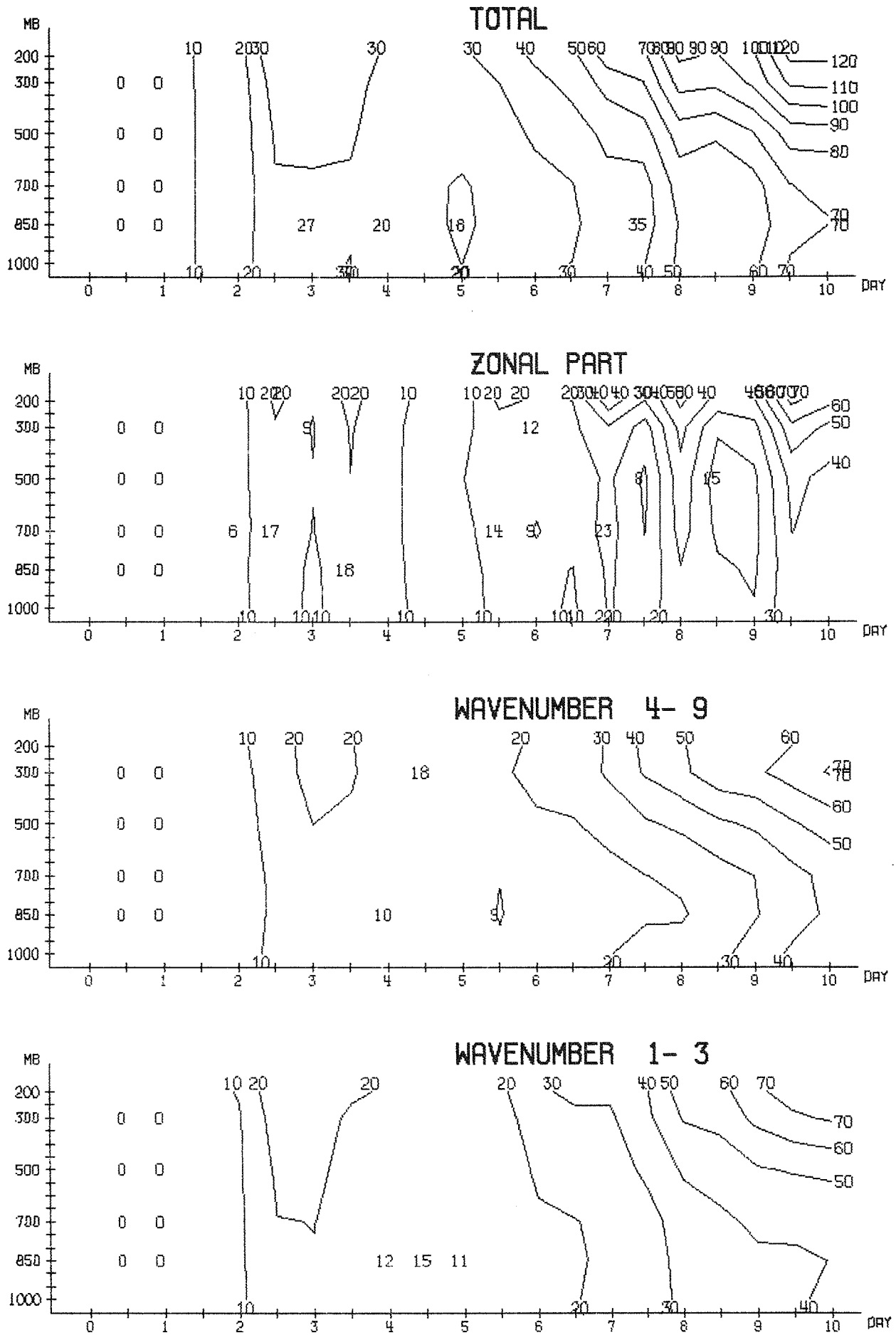

RMS-ERROR OF HEIGHT (M) MEAN BETWEEN 20.0 AND 82.5 N
RAD VS N48

Fig. 3.2.4

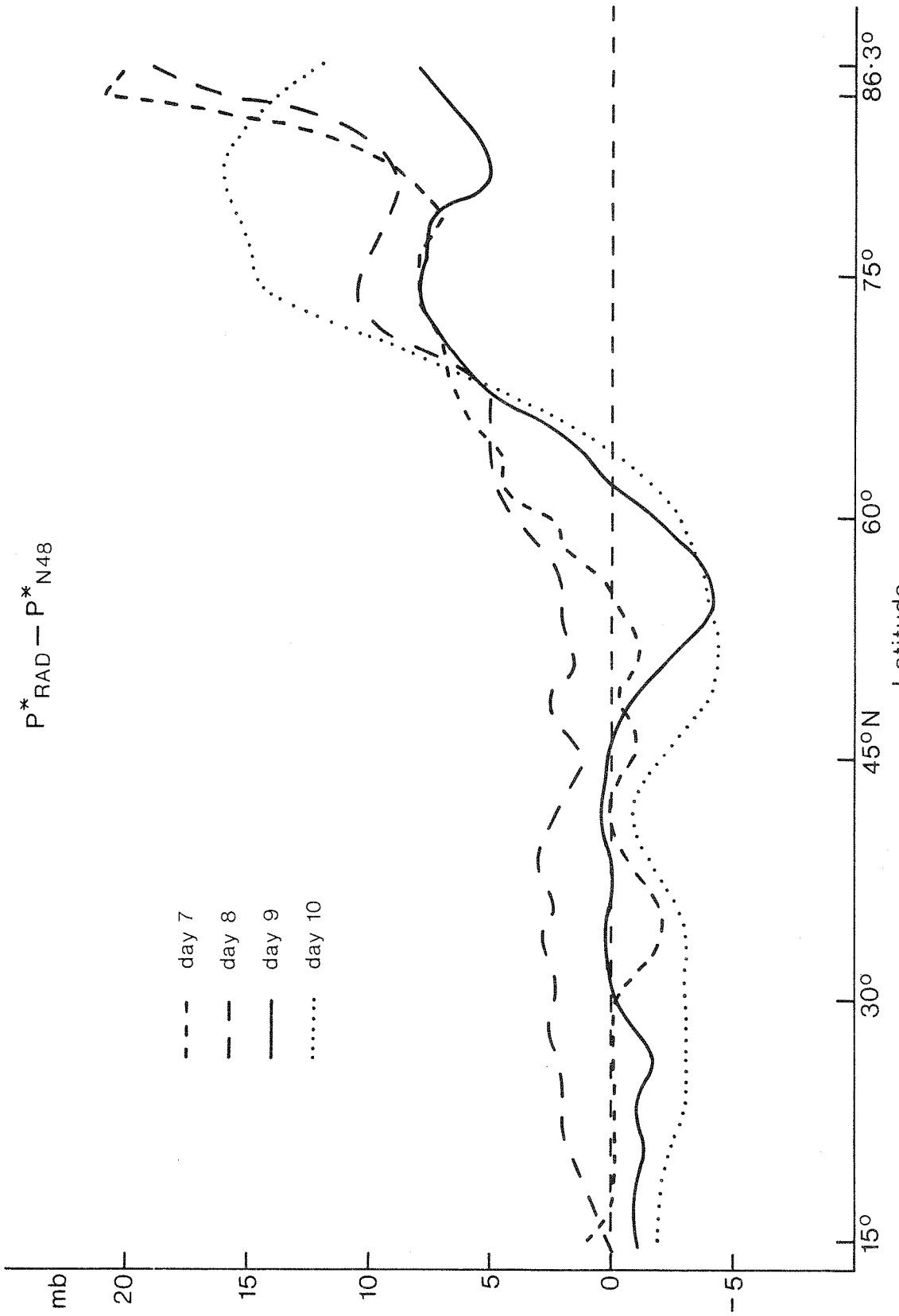

Fig. 3.2.5 Differences in zonal mean surface pressure at days 7 to 10 between the N48 and RAD runs.

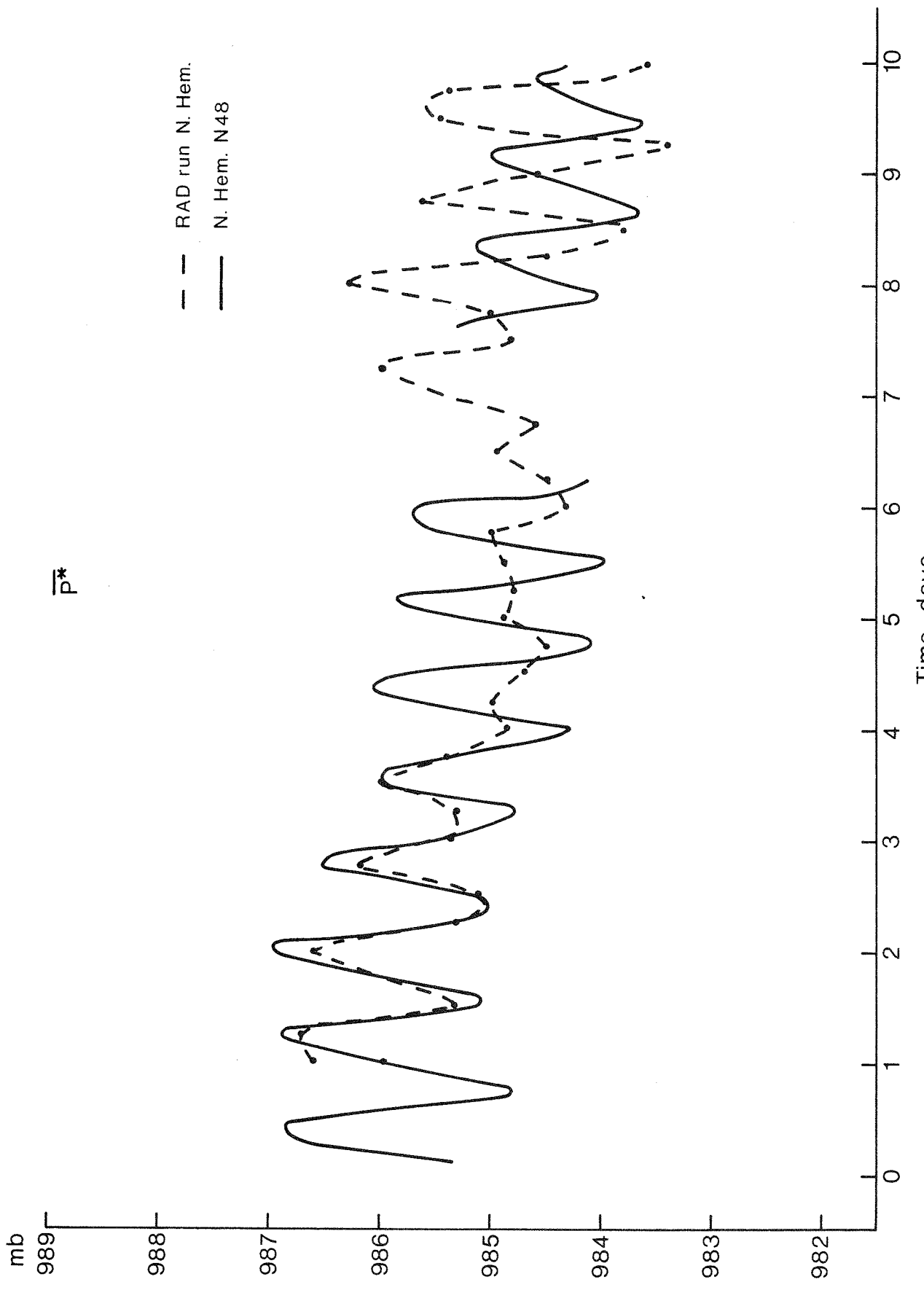

Fig. 3.2.6 Time evaluation of the mean surface pressure over the northern hemisphere for the N48 and RAD runs.

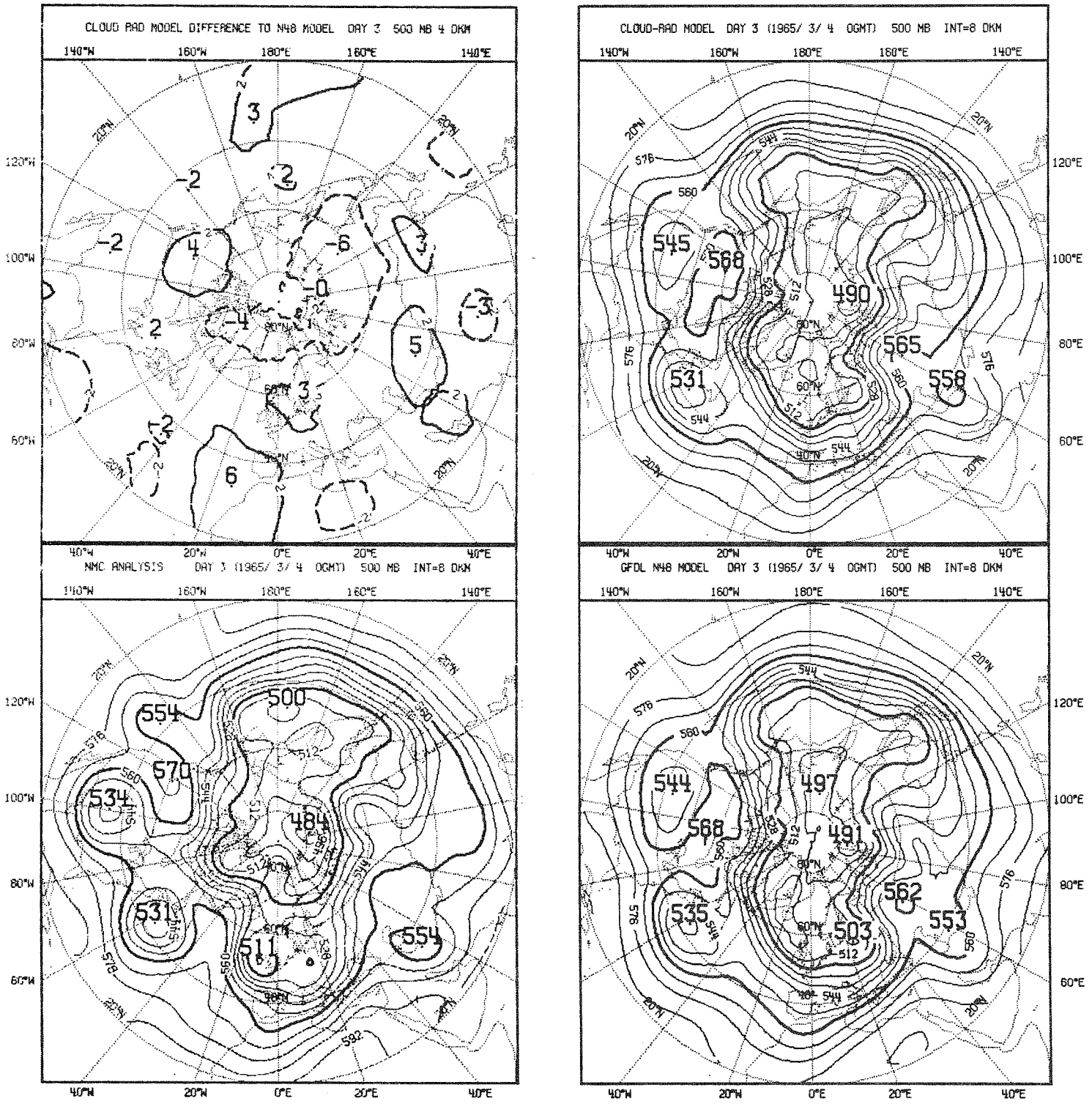

FIG. 3.3.1 BOTTOM LEFT : 500 MB NMC ANALYSIS. BOTTOM RIGHT : N48 FORECAST. TOP RIGHT : RAD FORECAST. TOP LEFT : DIFFERENCES BETWEEN THE FORECASTS FOR 00Z MARCH 4 1965.

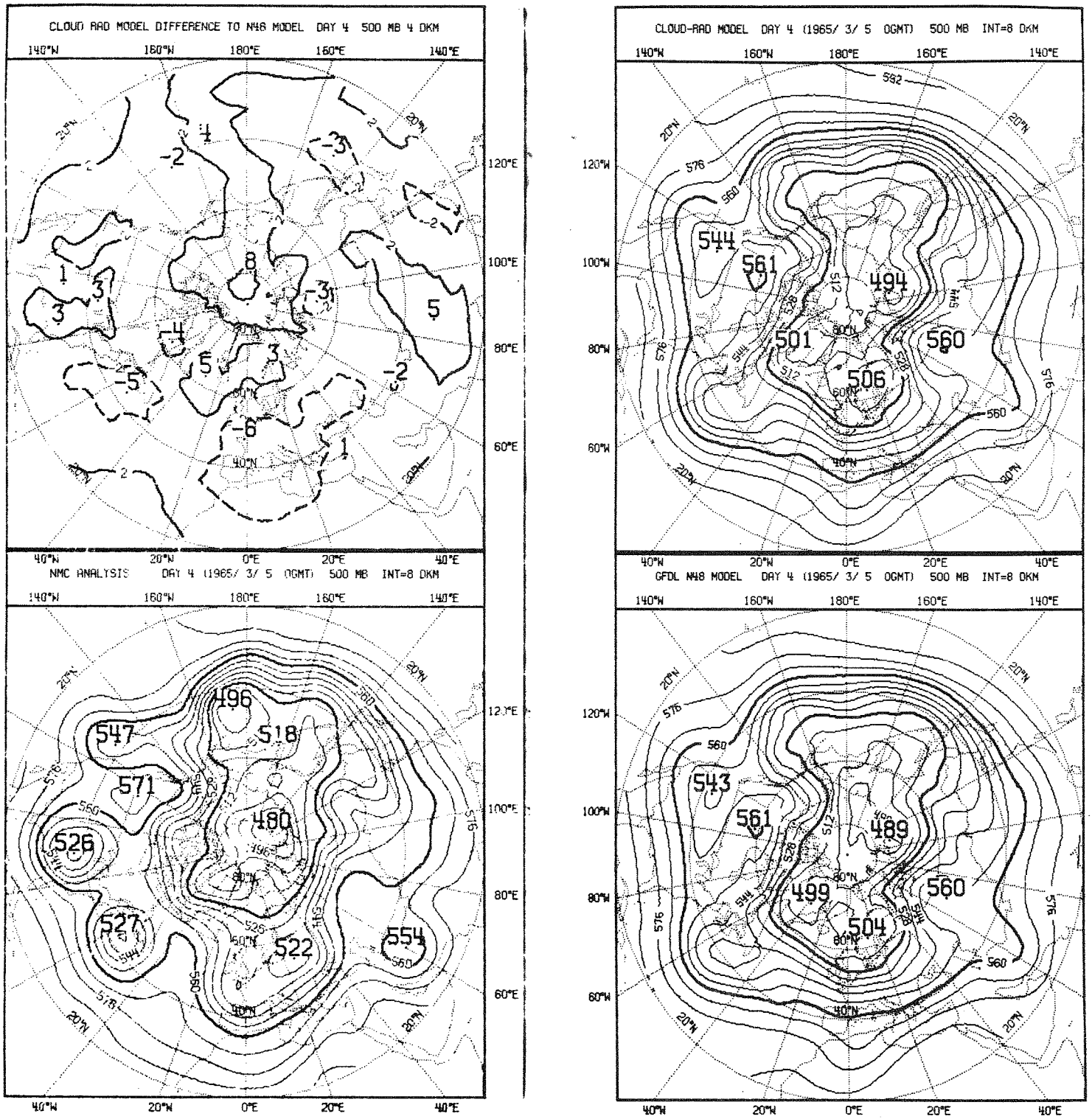

FIG. 3.3.2 BOTTOM LEFT : 500 MB NMC ANALYSIS BOTTOM RIGHT : N48 FORECAST TOP RIGHT : RAD FORECAST TOP LEFT : DIFFERENCES BETWEEN THE FORECASTS FOR 00Z MARCH 5 1965.

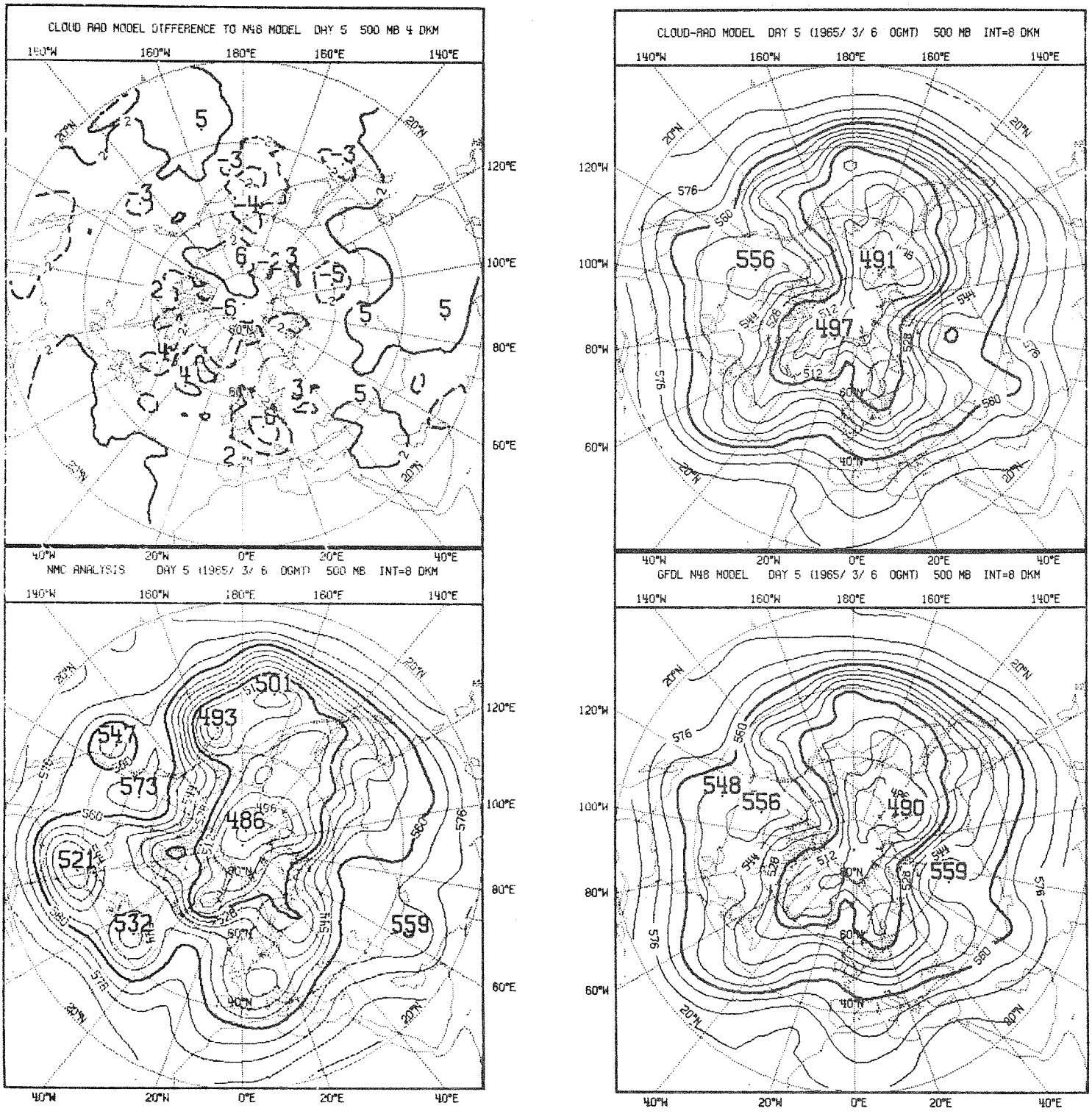

FIG. 3.3.3 BOTTOM LEFT : 500 MB NMC ANALYSIS. BOTTOM RIGHT : N48 FORECAST. TOP RIGHT : RAD FORECAST. TOP LEFT : DIFFERENCES BETWEEN THE FORECASTS FOR 00Z MARCH 6 1965.

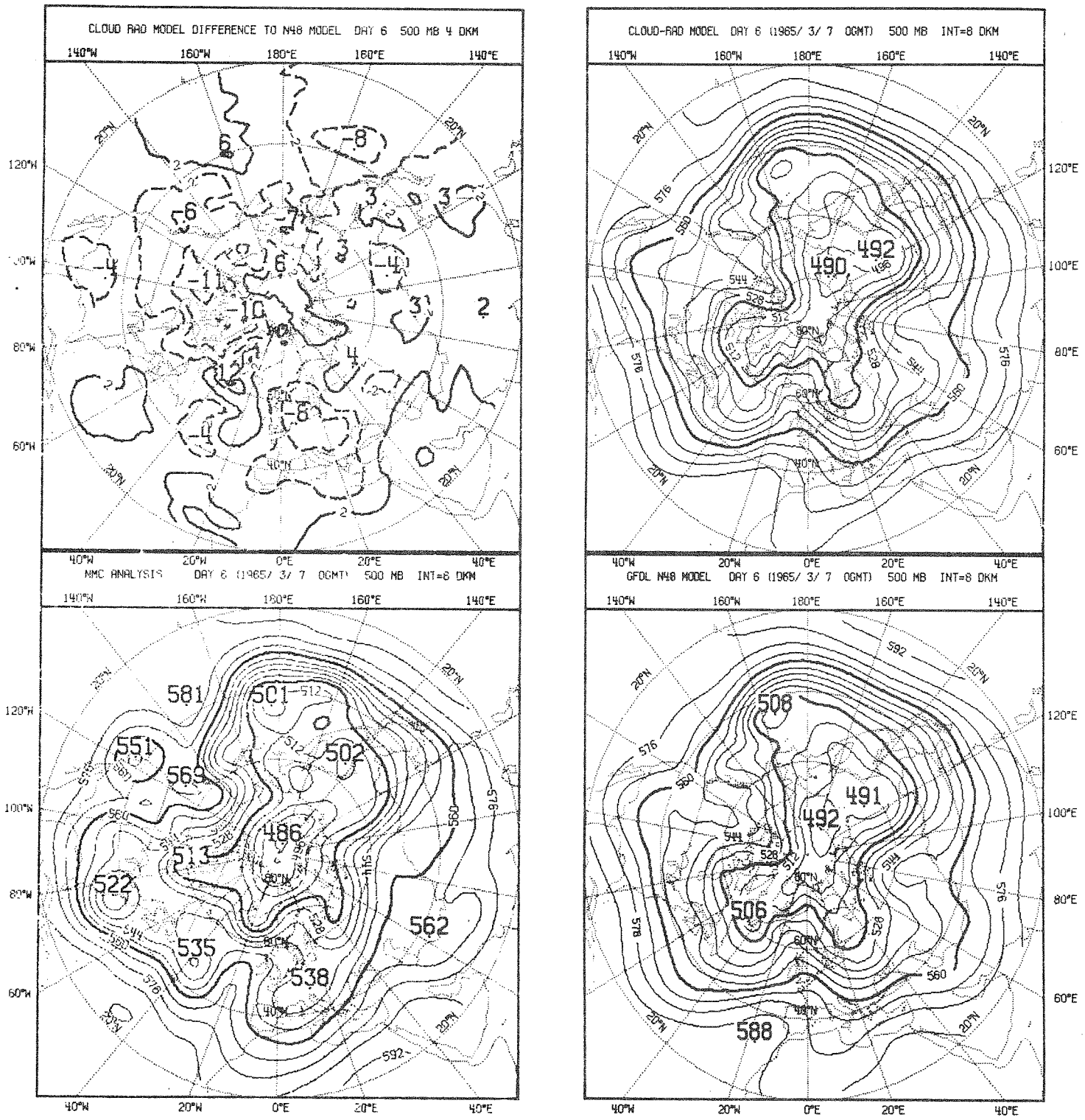

FIG. 3.3.4 BOTTOM LEFT : 500 MB NMC ANALYSIS. BOTTOM RIGHT : N48 FORECAST. TOP RIGHT : RAD FORECAST. TOP LEFT FOR 00Z MARCH 7 1965.

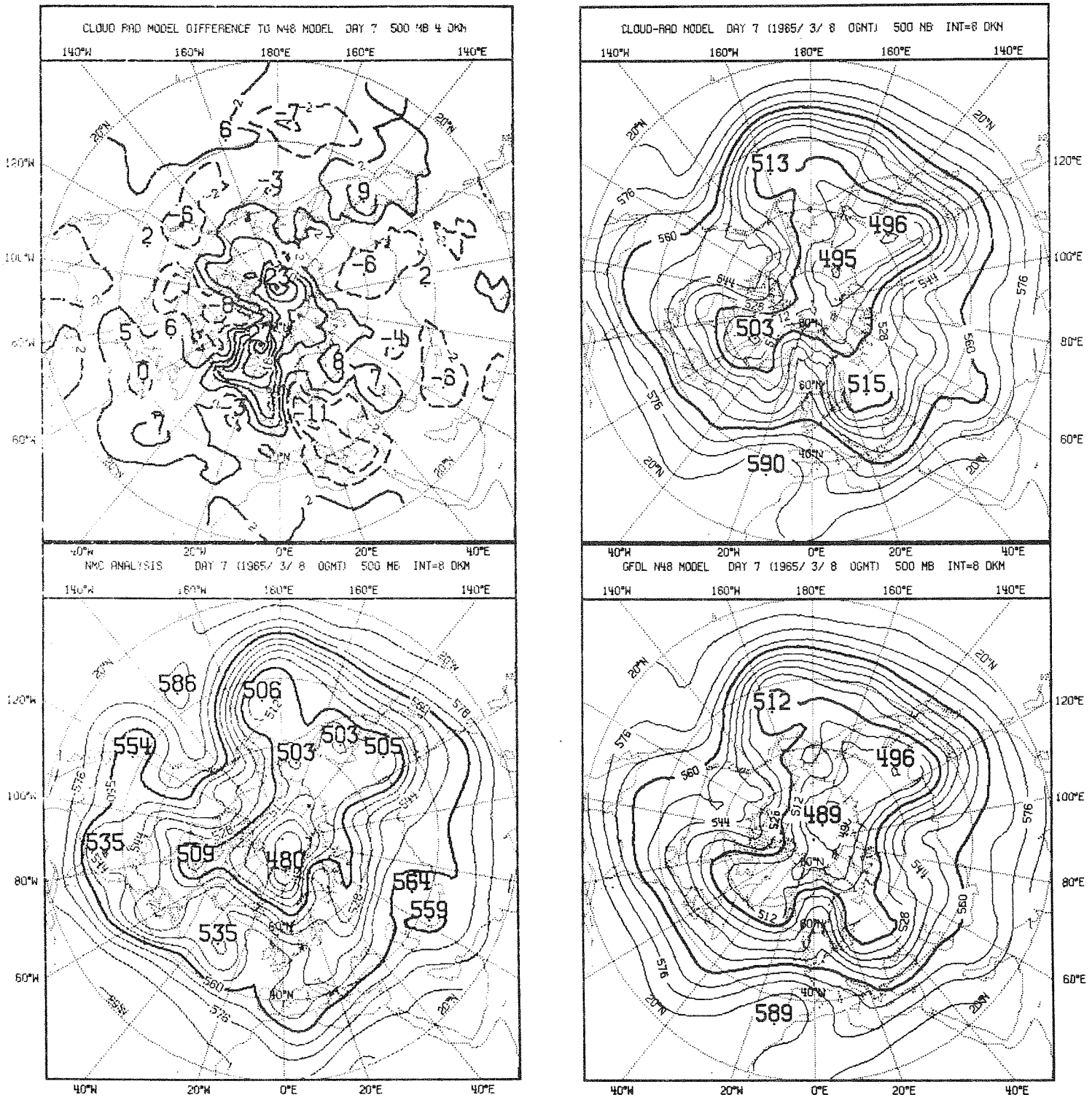

FIG. 3.3.5 BOTTOM LEFT : 500 MB NMC ANALYSIS. BOTTOM RIGHT : N48 FORECAST. TOP RIGHT : RAD FORECAST. TOP LEFT : DIFFERENCES BETWEEN THE FORECASTS FOR 00Z MARCH 8 1965.

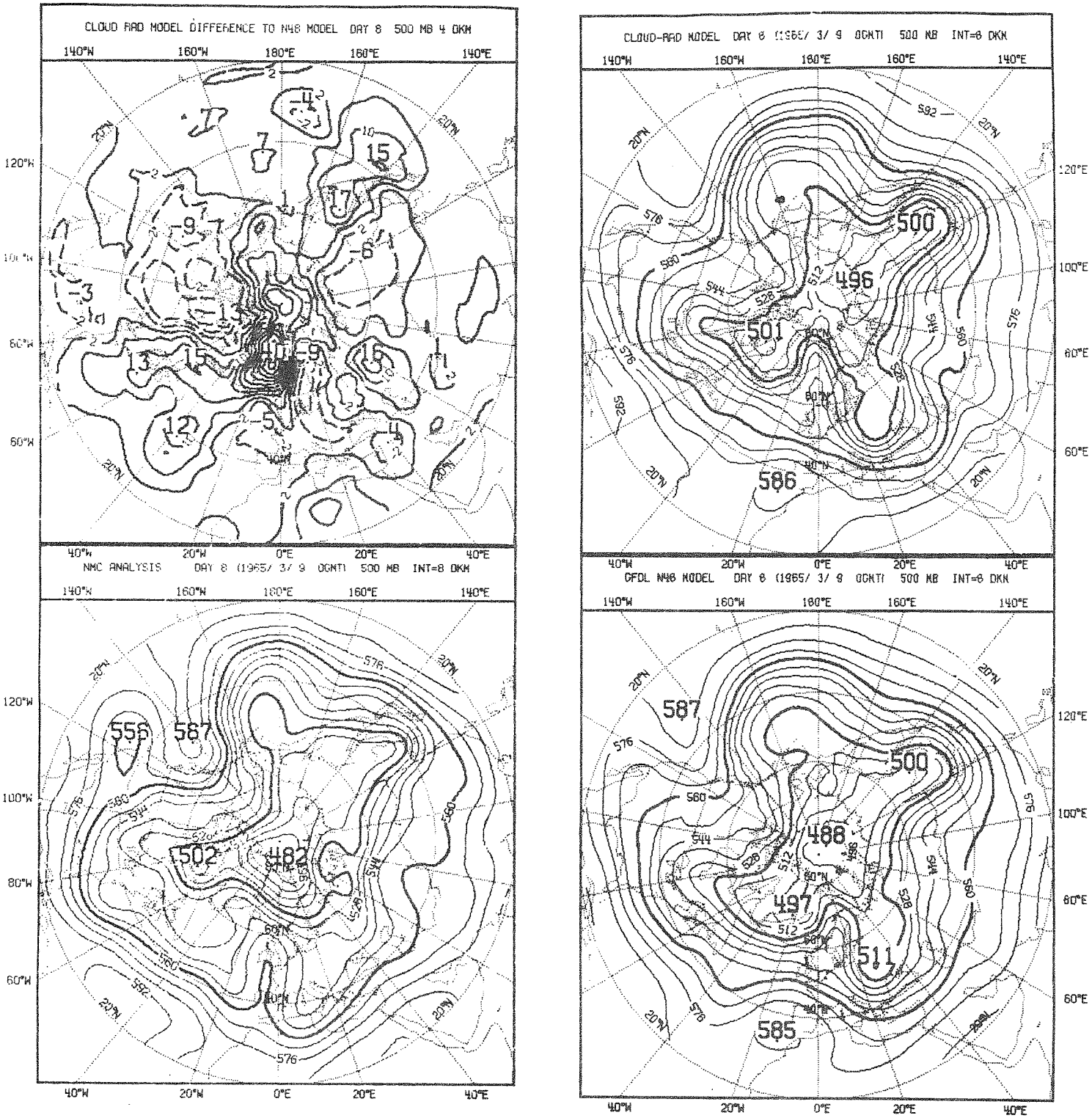

FIG. 3.3.6 BOTTOM LEFT : 500 MB NMC ANALYSIS. BOTTOM RIGHT : N48 FORECAST. TOP RIGHT : RAD FORECAST. TOP LEFT : DIFFERENCES BETWEEN THE FORECASTS FOR 00Z MARCH 9 1965.

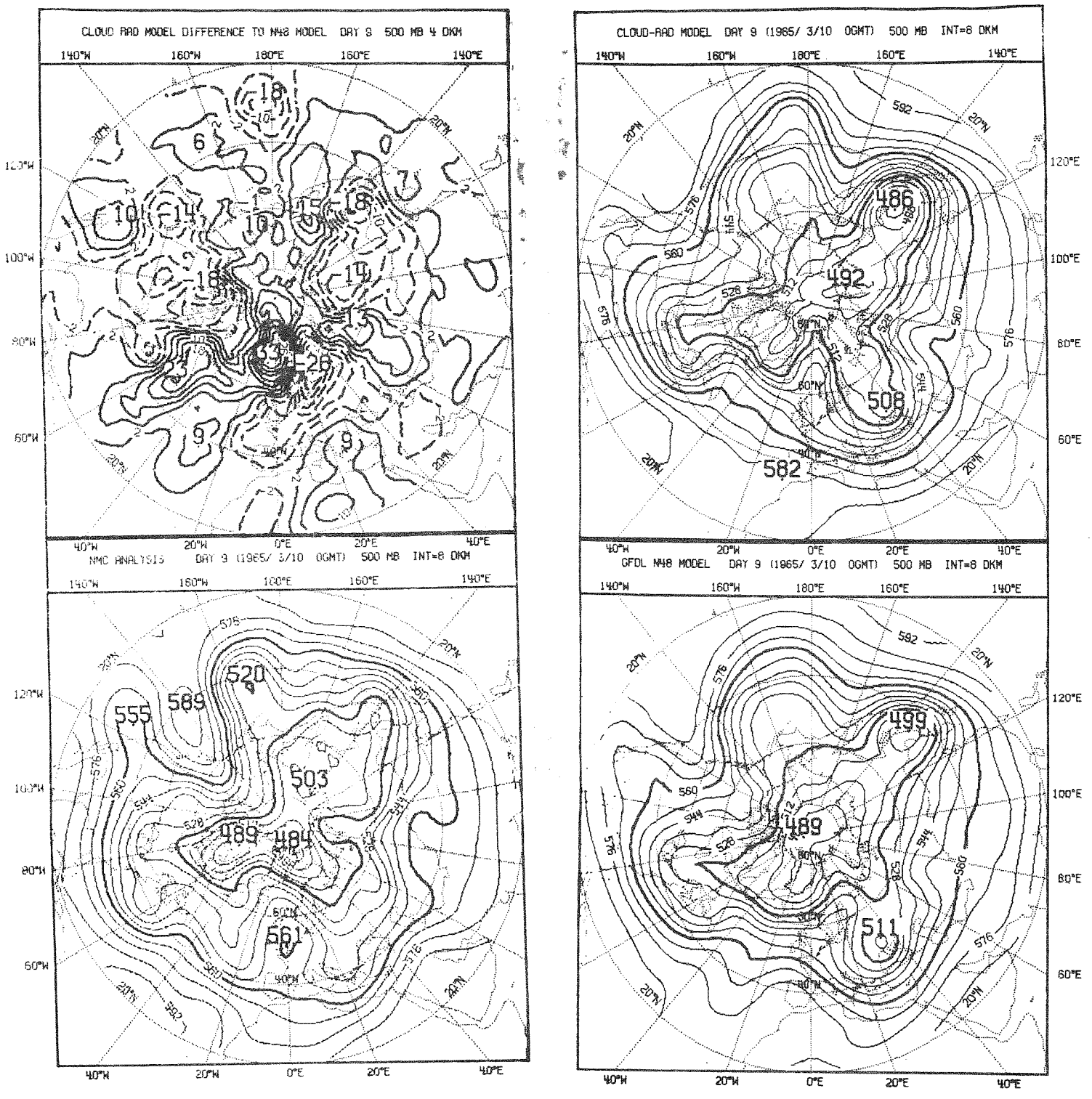

FIG. 3.3.7 BOTTOM LEFT : 500 MB NMC ANALYSIS. BOTTOM RIGHT : N48 FORECAST. TOP RIGHT : RAD FORECAST. TOP LEFT : DIFFERENCES BETWEEN THE FORECASTS FOR 00Z MARCH 10 1965.

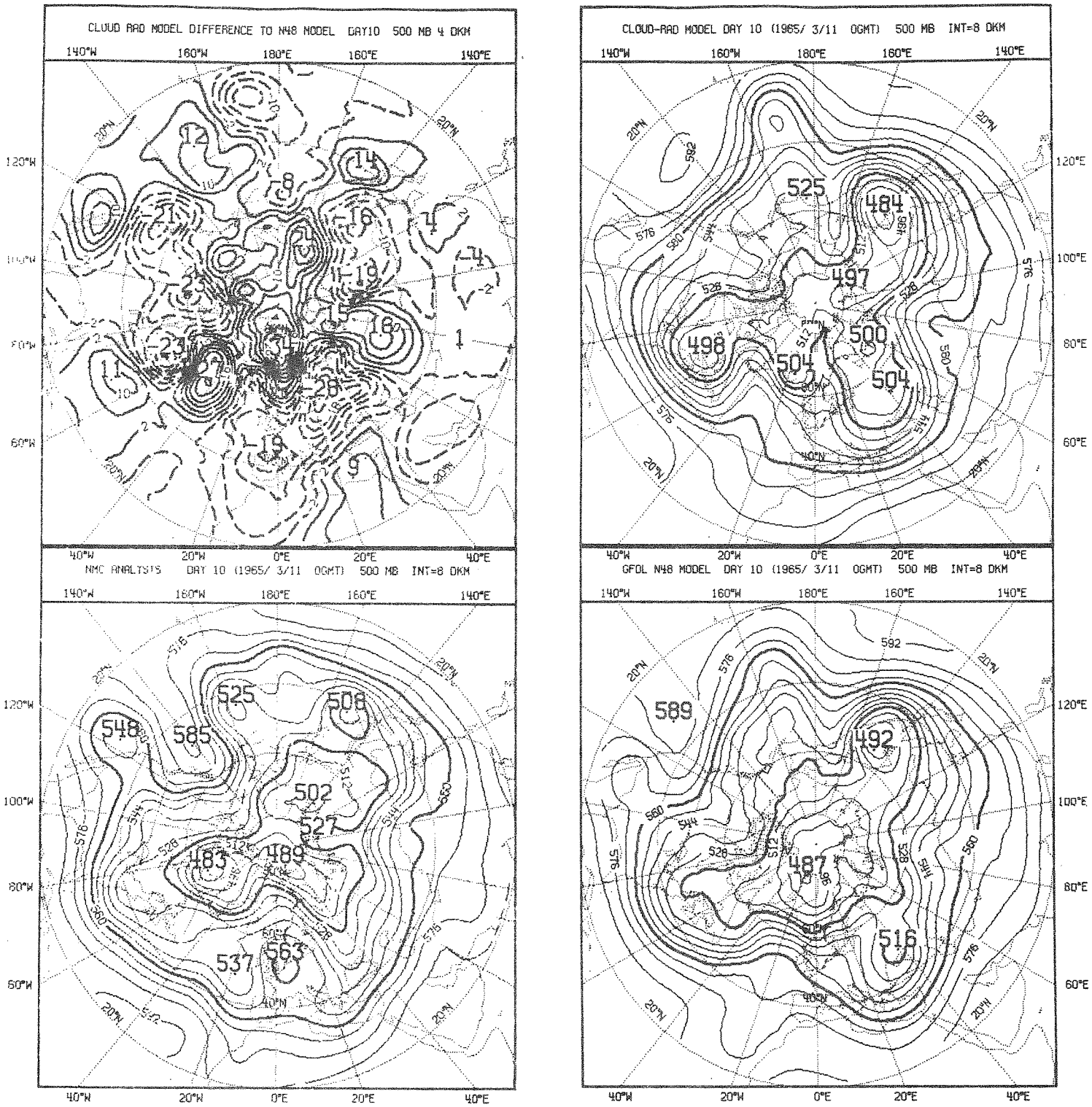

FIG. 3.3.8 BOTTOM LEFT : 500 MB NMC ANALYSIS. BOTTOM RIGHT : N48 FORECAST. TOP RIGHT : RAD FORECAST. TOP LEFT : DIFFERENCES BETWEEN THE FORECASTS FOR 00Z MARCH 11 1965.

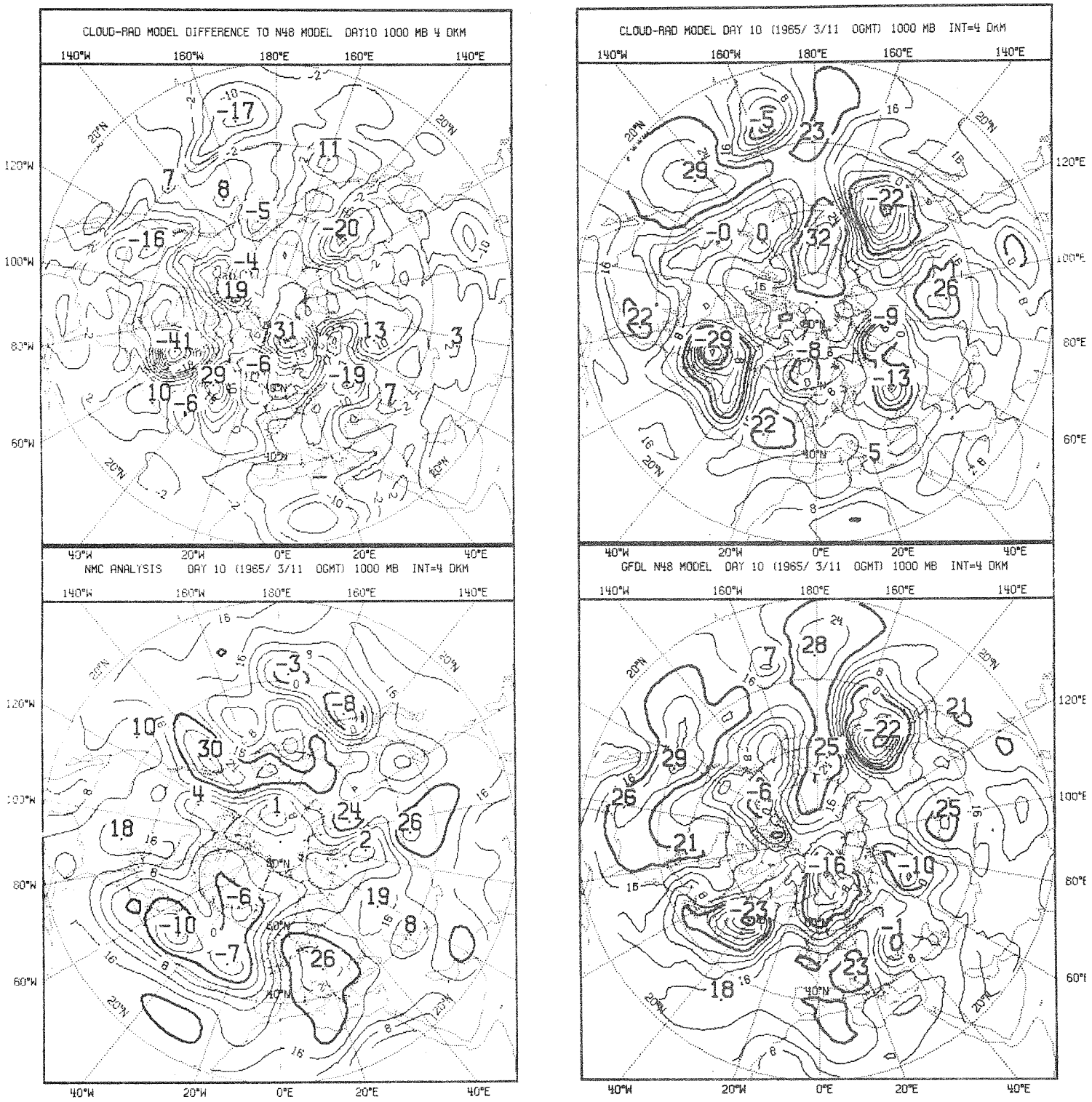

FIG. 3.3.9 BOTTOM LEFT : 1000 MB NMC ANALYSIS. BOTTOM RIGHT : N48 FORECAST. TOP RIGHT : RA FORECAST. TOP LEFT : DIFFERENCES BETWEEN THE FORECASTS FOR 00Z MARCH 11 1965.

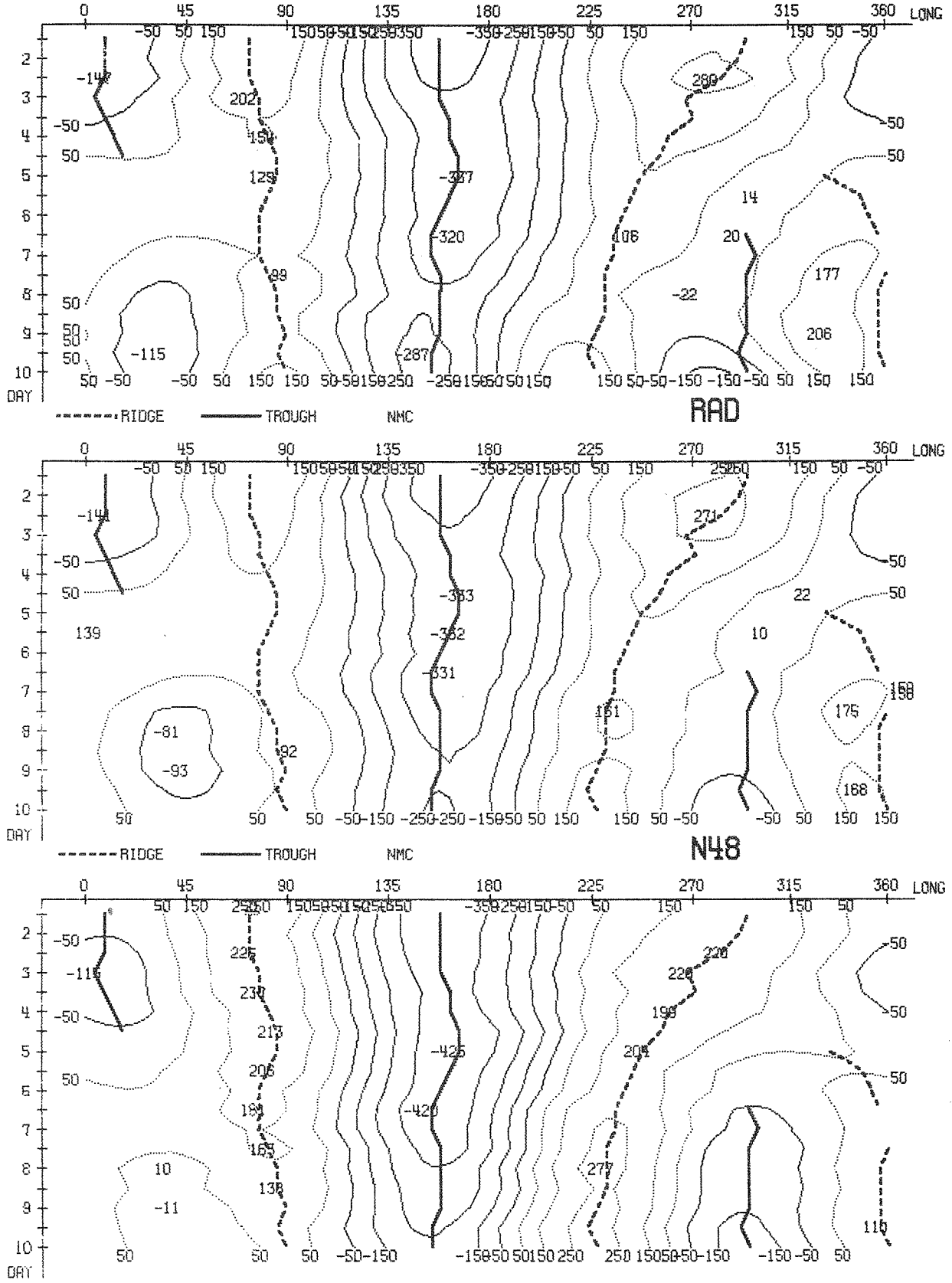

Fig. 3.3.10 Hovmöller diagram of 500 mb geopotential for wave numbers 1-3 at 50N in RAD (top) N48 (centre) and NMC (bottom). The trough lines (solid) and ridge lines (dashed) on the NMC analysis have been copied onto the forecast charts.

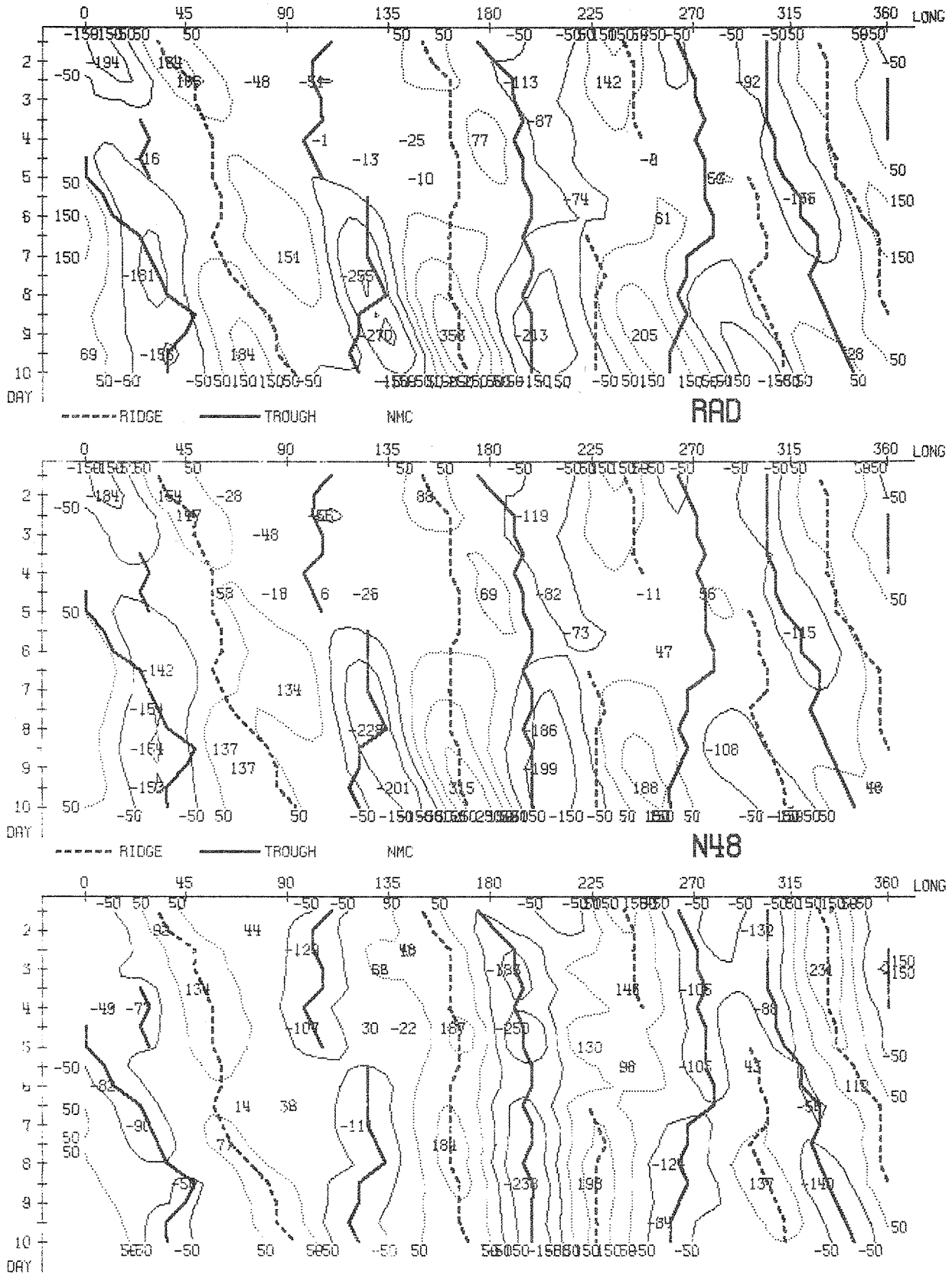

Fig. 3.3.11 Hovmöller diagram of 500 mb geopotential for RAD (top) N48 (centre) and NMC (bottom). The trough wave numbers 4-9 at 50N in lines (solid) and ridge lines (dashed) on the NMC analysis have been copied onto the forecast charts.

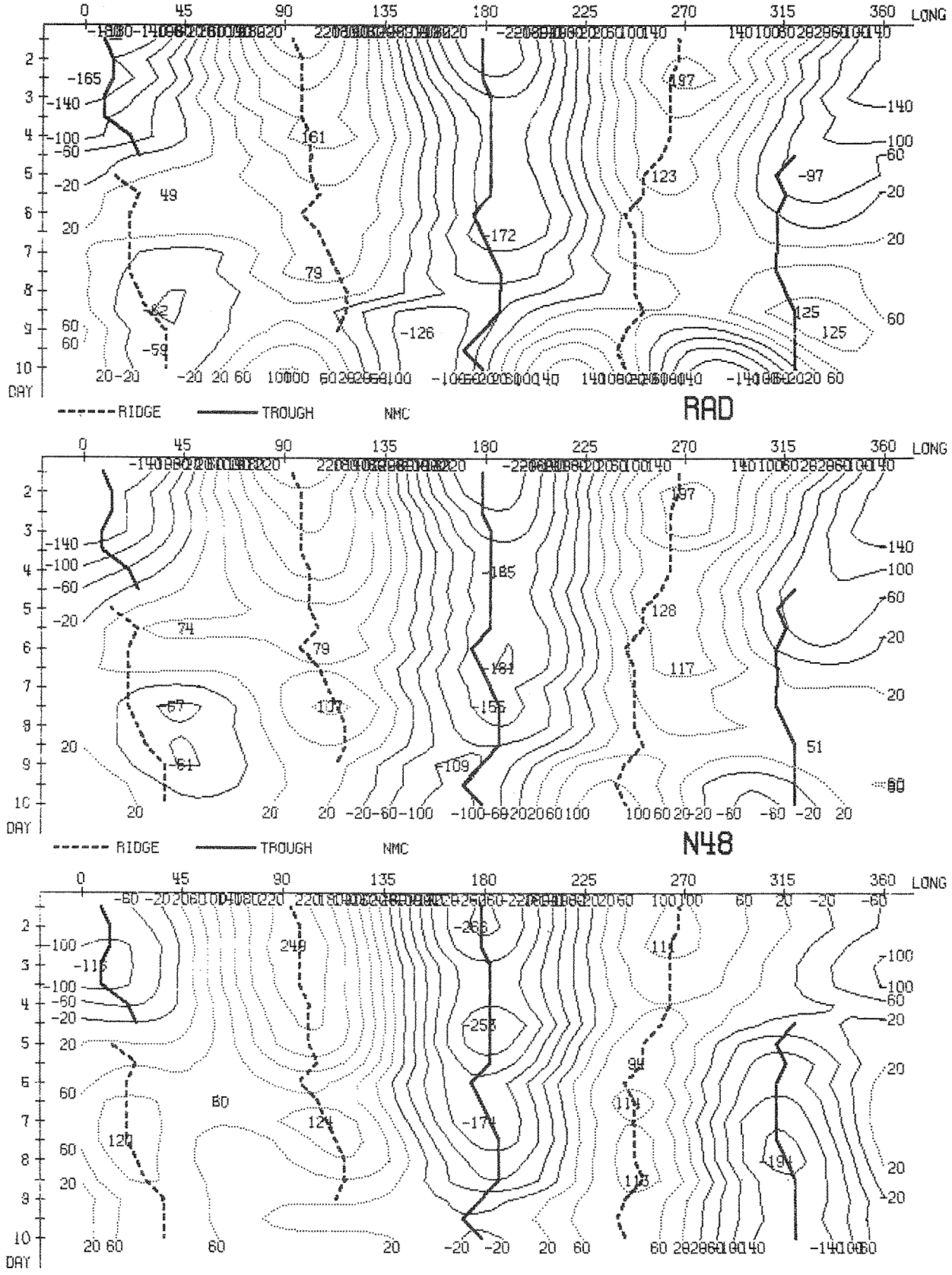

Fig. 3.3.12 Hovmöller diagram of 1000 mb geopotential for wave numbers 1-3 at 50N in RAD (top) N48 (centre) and NMC (bottom). The trough lines (solid) and ridge lines (dashed) on the NMC analysis have been copied onto the forecast charts.

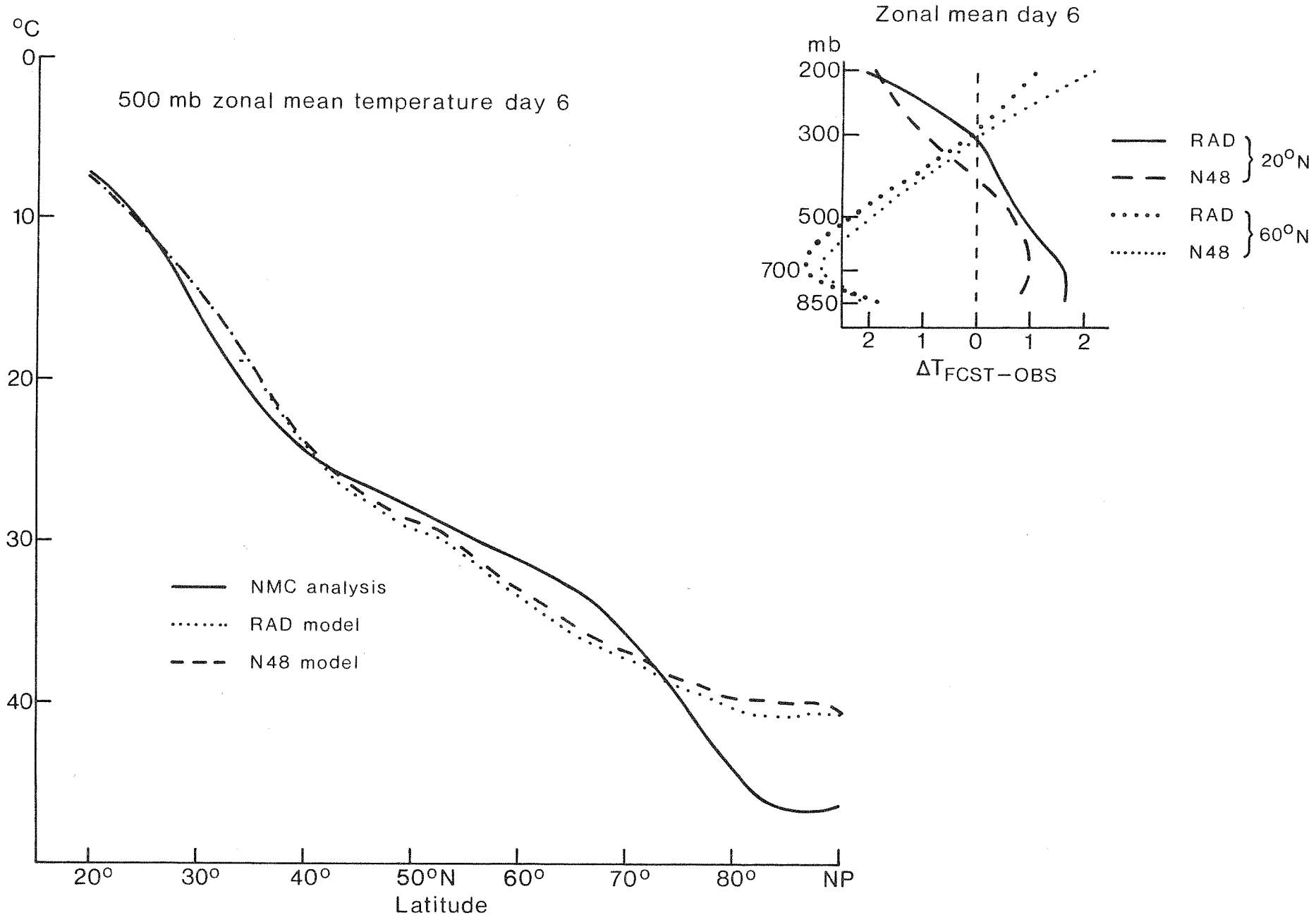

Fig. 3.3.13 Zonal mean of 500 mb temperature at day 6 in NMC analysis, RAD and N48 runs. The inset shows the vertical structure of the differences between the forecasts and observation of the zonal mean temperatures at 20°N and 60°N.

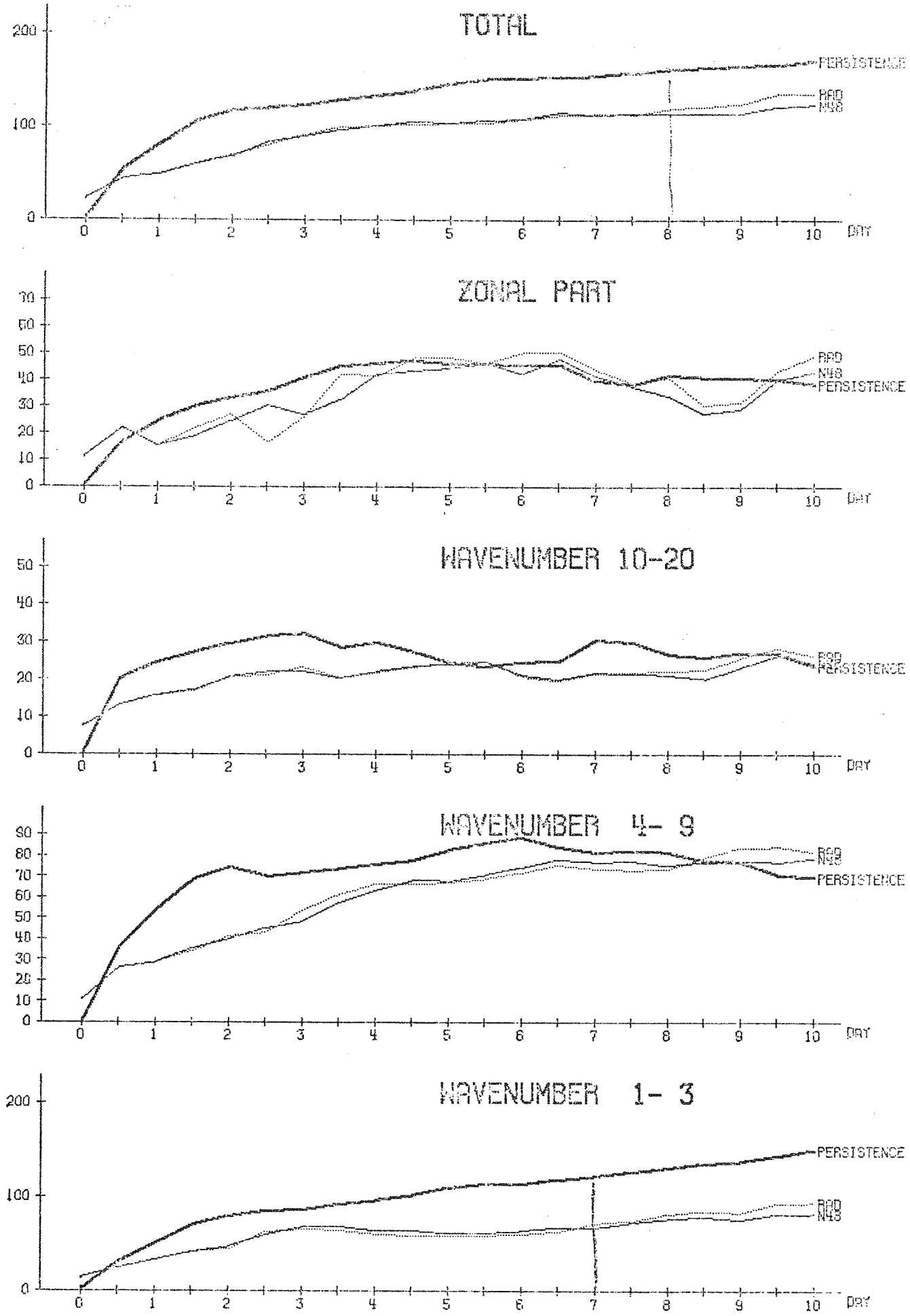

Fig. 3.4.1 Time evolution of R.M.S. geopotential height errors for RAD, N48, and persistence for the troposphere (200 - 1000 mb) north of 20N by wave number groups. The dotted lines show level of the climatological variance.

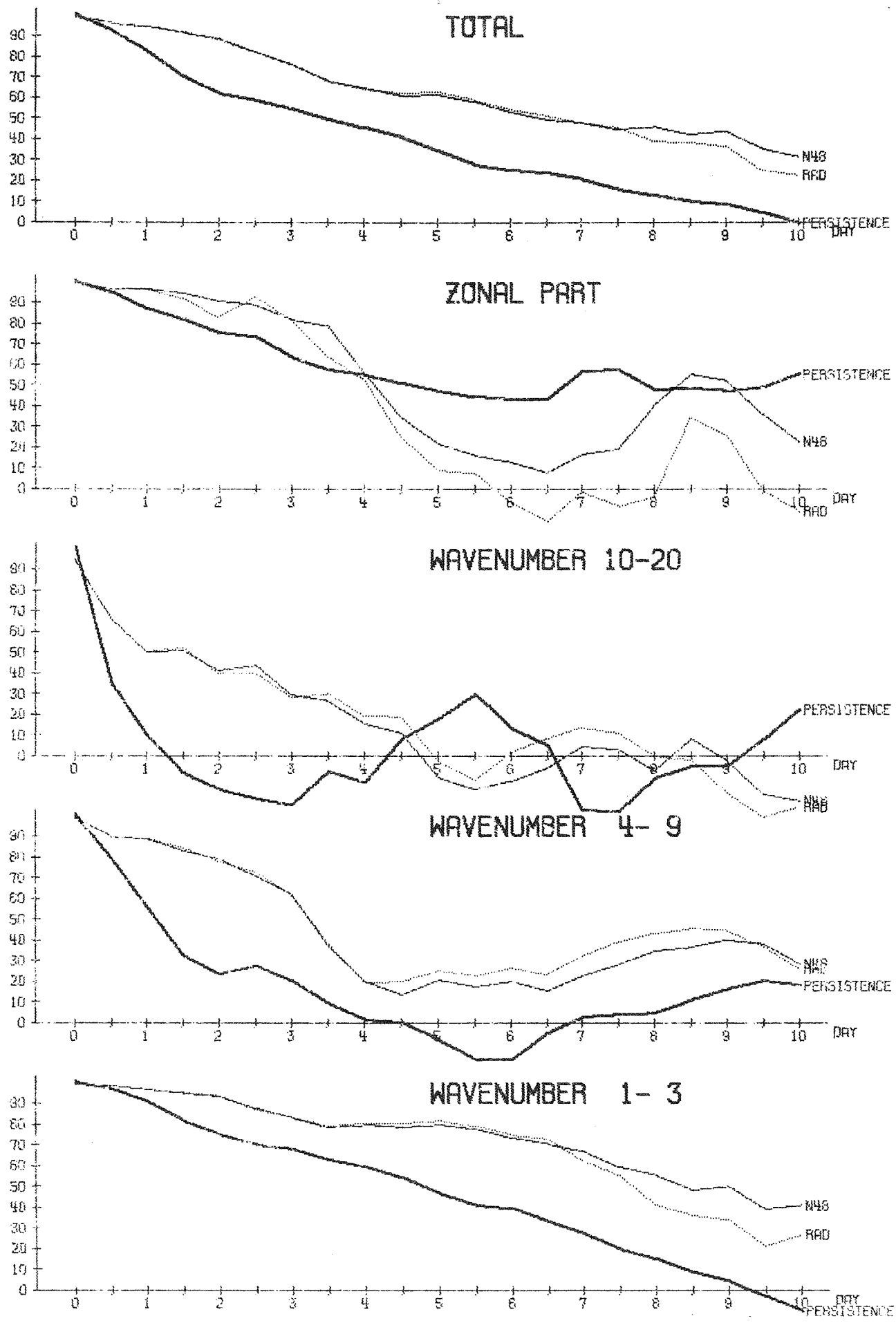

Fig. 3.4.2 Time evolution of geopotential anomaly correlation coefficient for the same volume and the same runs as fig. 3.4.1

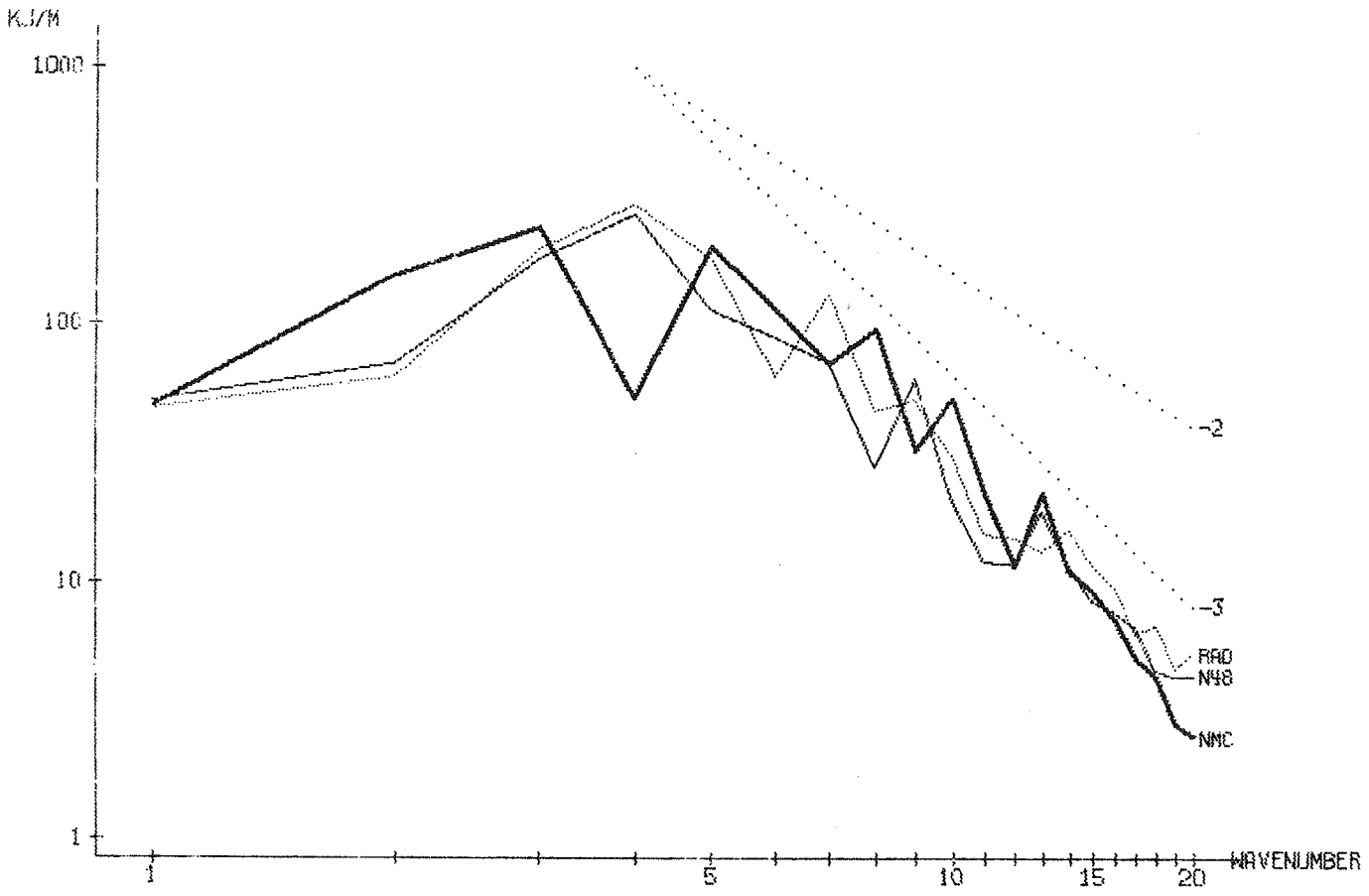

Fig. 3.5.1 Spectra of kinetic energy averaged over the region 200 - 1000 mb and 40N to 60N and the period days 7½ to 10.

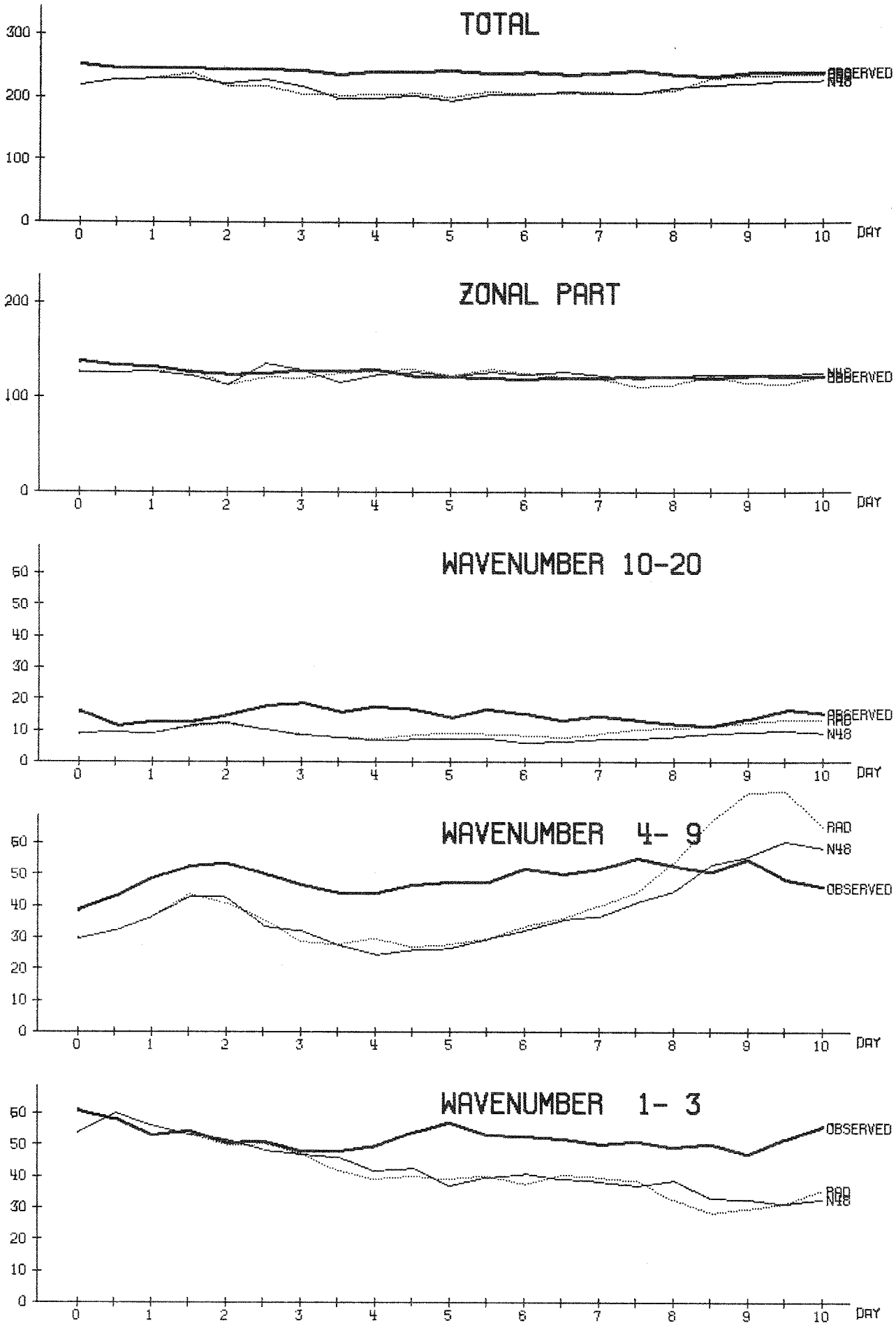

Fig. 3.5.2 Time evolution of kinetic energy for the troposphere north of 20N by wave number groups.

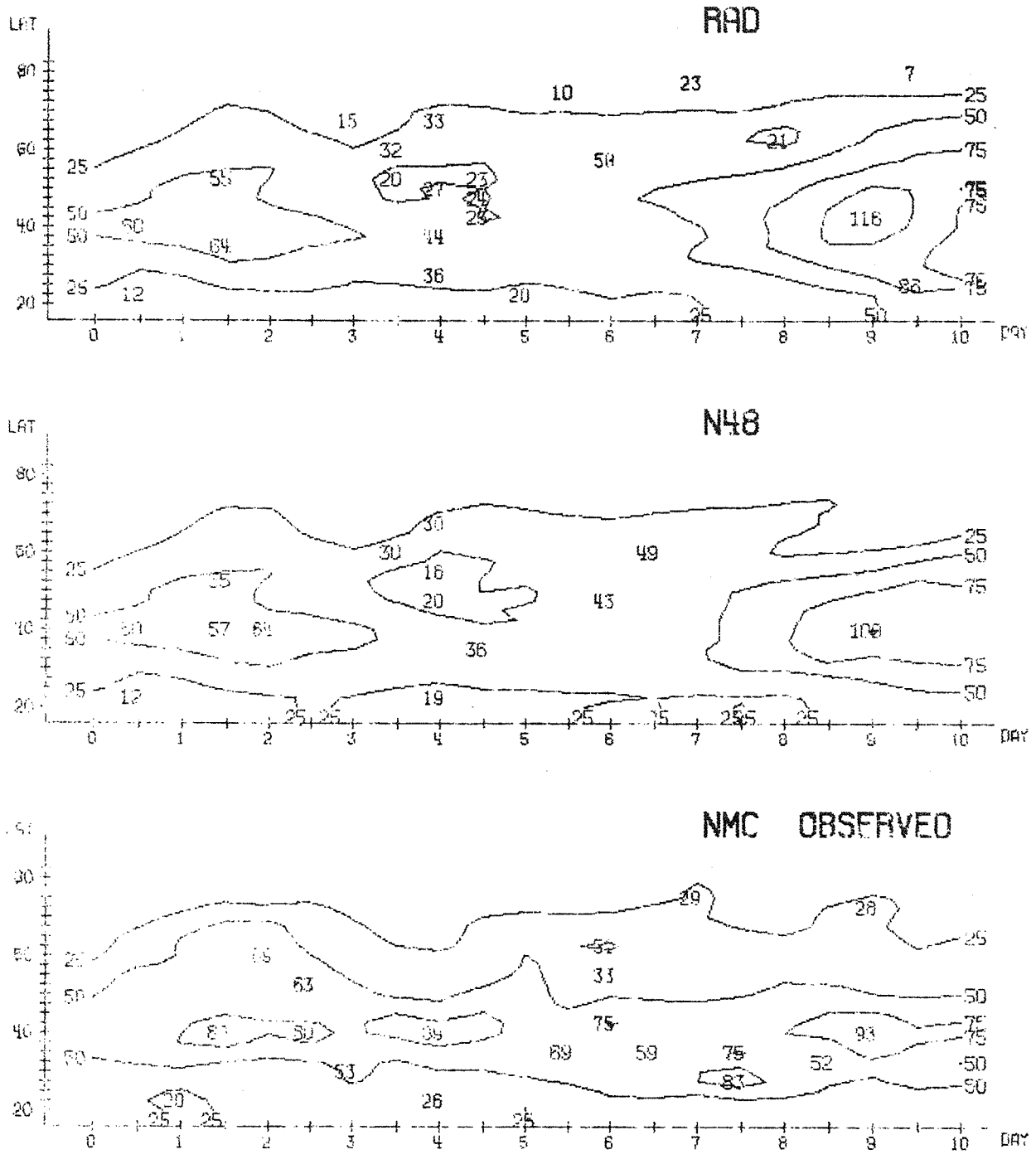

Fig. 3.5.3 Latitude time diagram of the vertically integrated eddy kinetic energy for RAD and N48 runs and for NMC analysis.

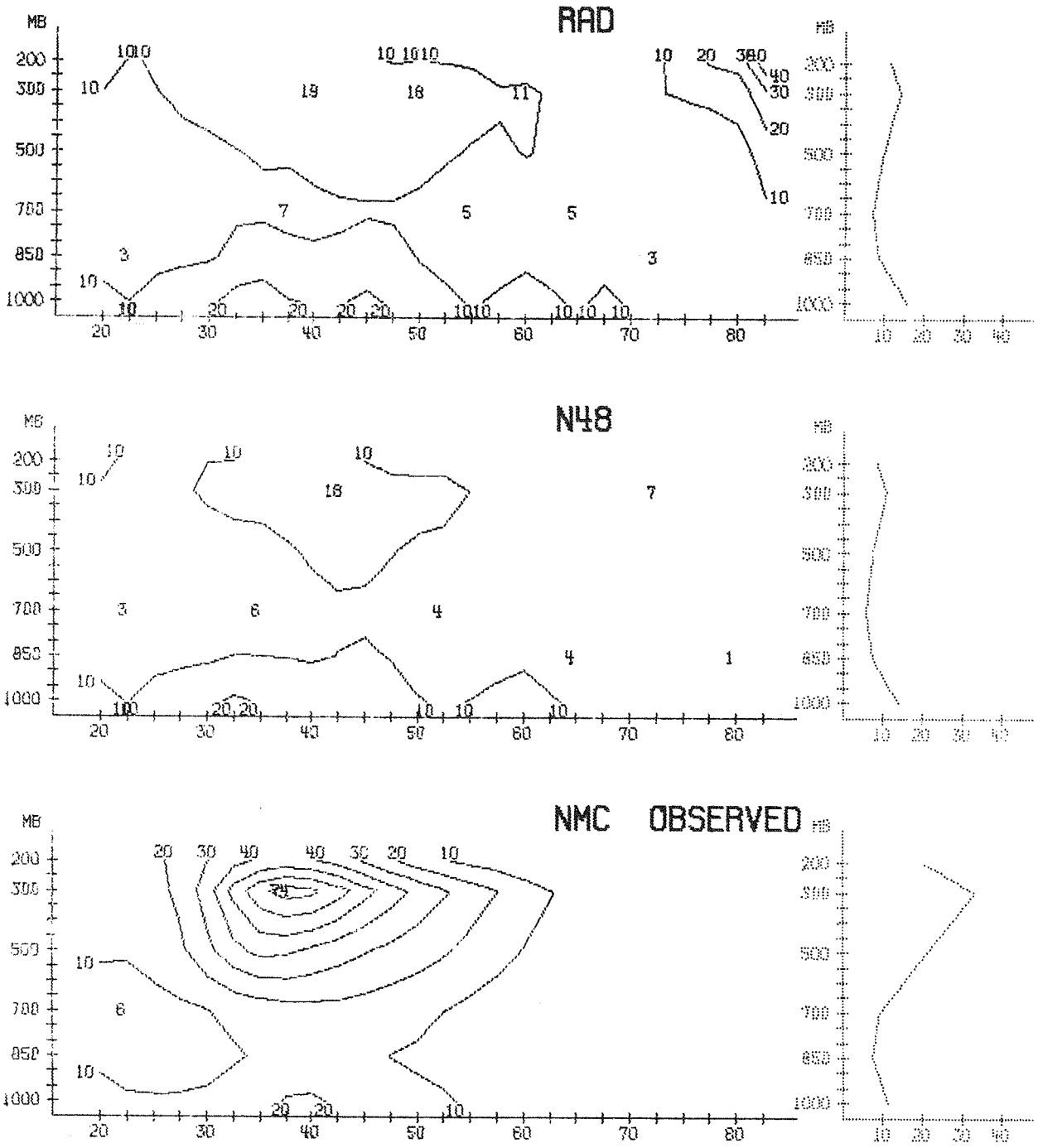

Fig. 3.5.4 Latitude height cross-section of the eddy kinetic energy in wave numbers 10-20 averaged over days 4½ runs and for the observations. The small panels at the right show the vertical profile of the meridional integral.

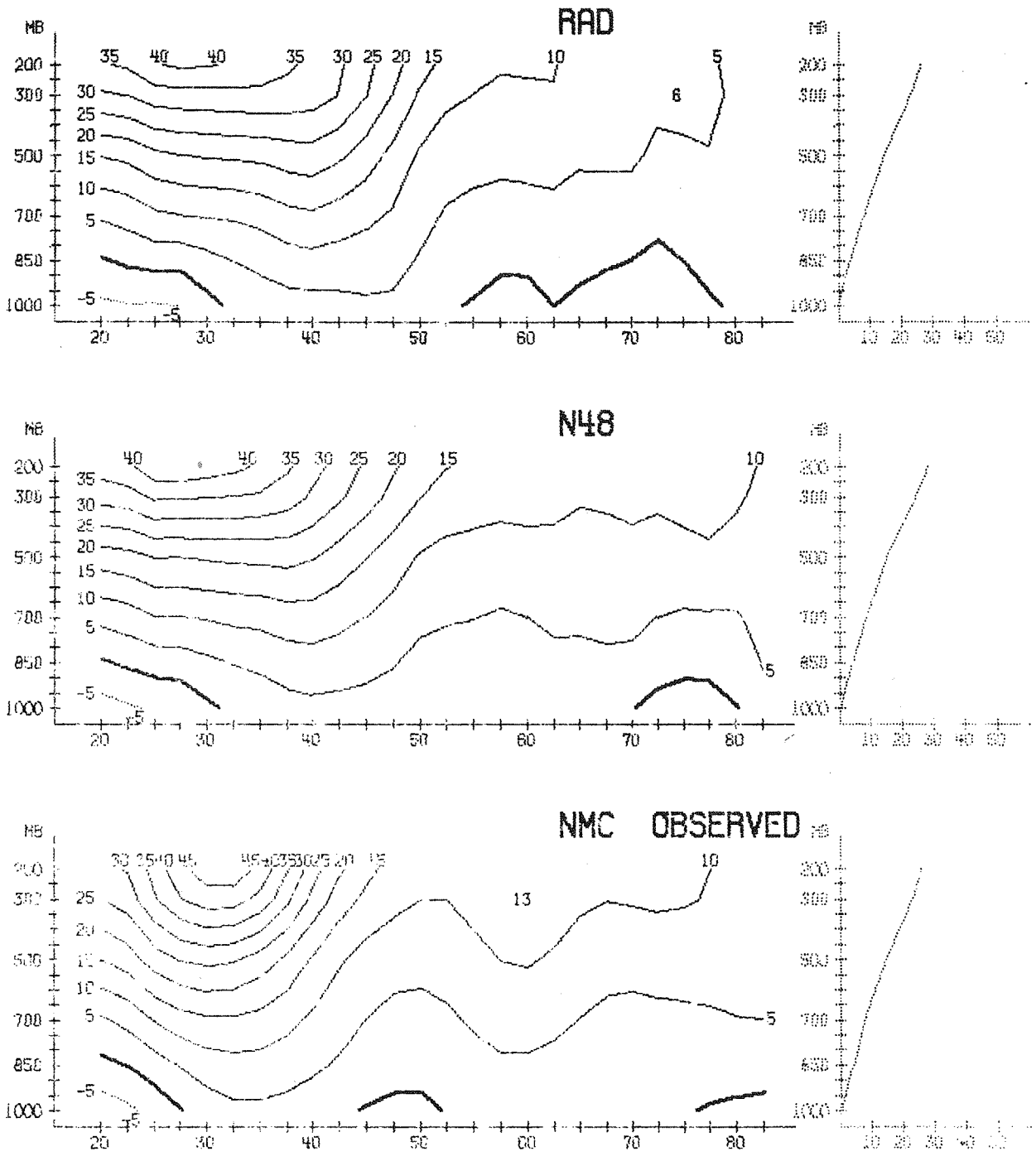

Fig. 3.5.5 Zonal mean of zonal wind averaged over days 7½ to 10. The panels on the right show the meridional integral.

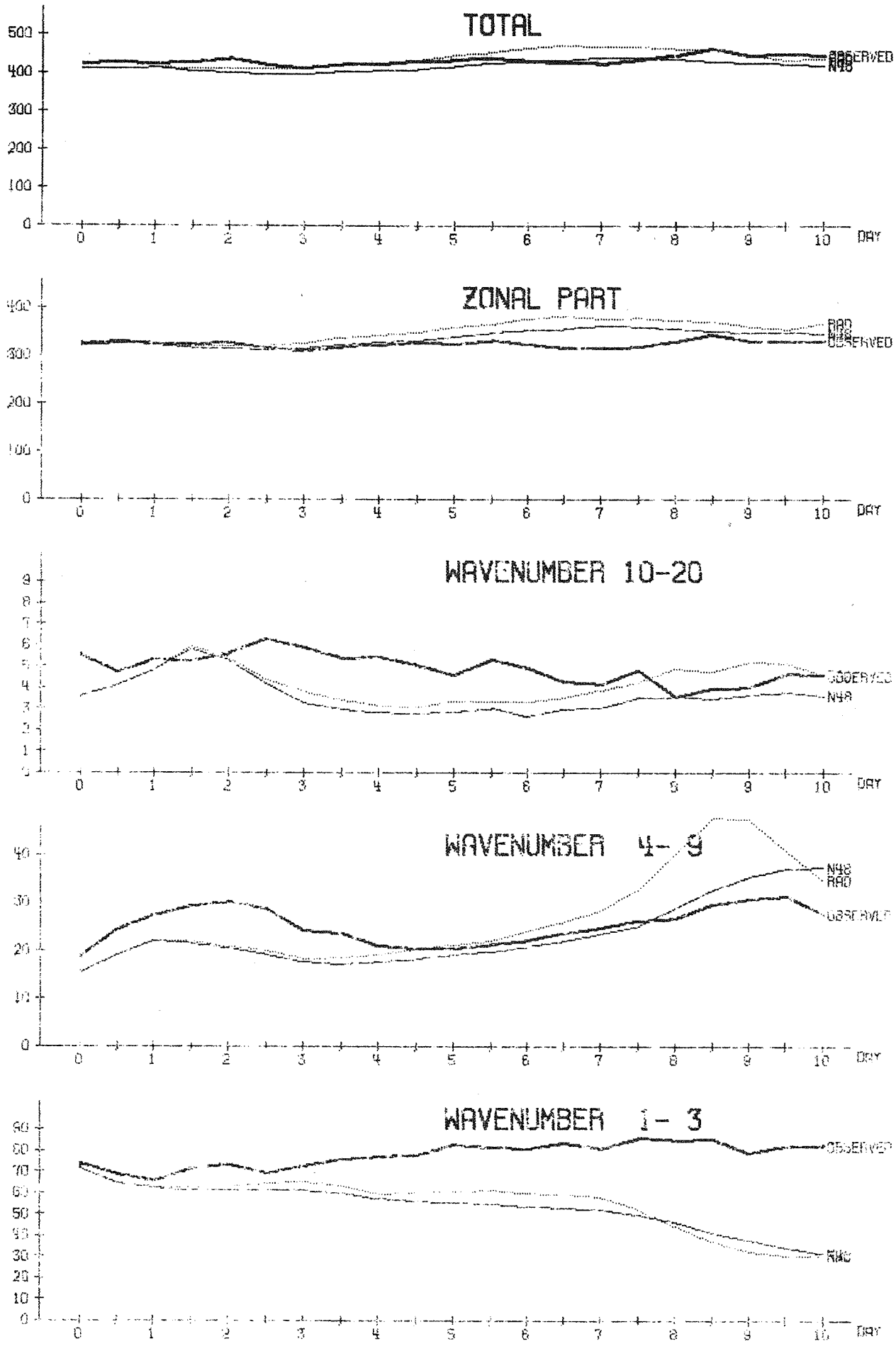

Fig. 3.5.6 Time evolution of the available potential energy averaged over the troposphere north of 20N.

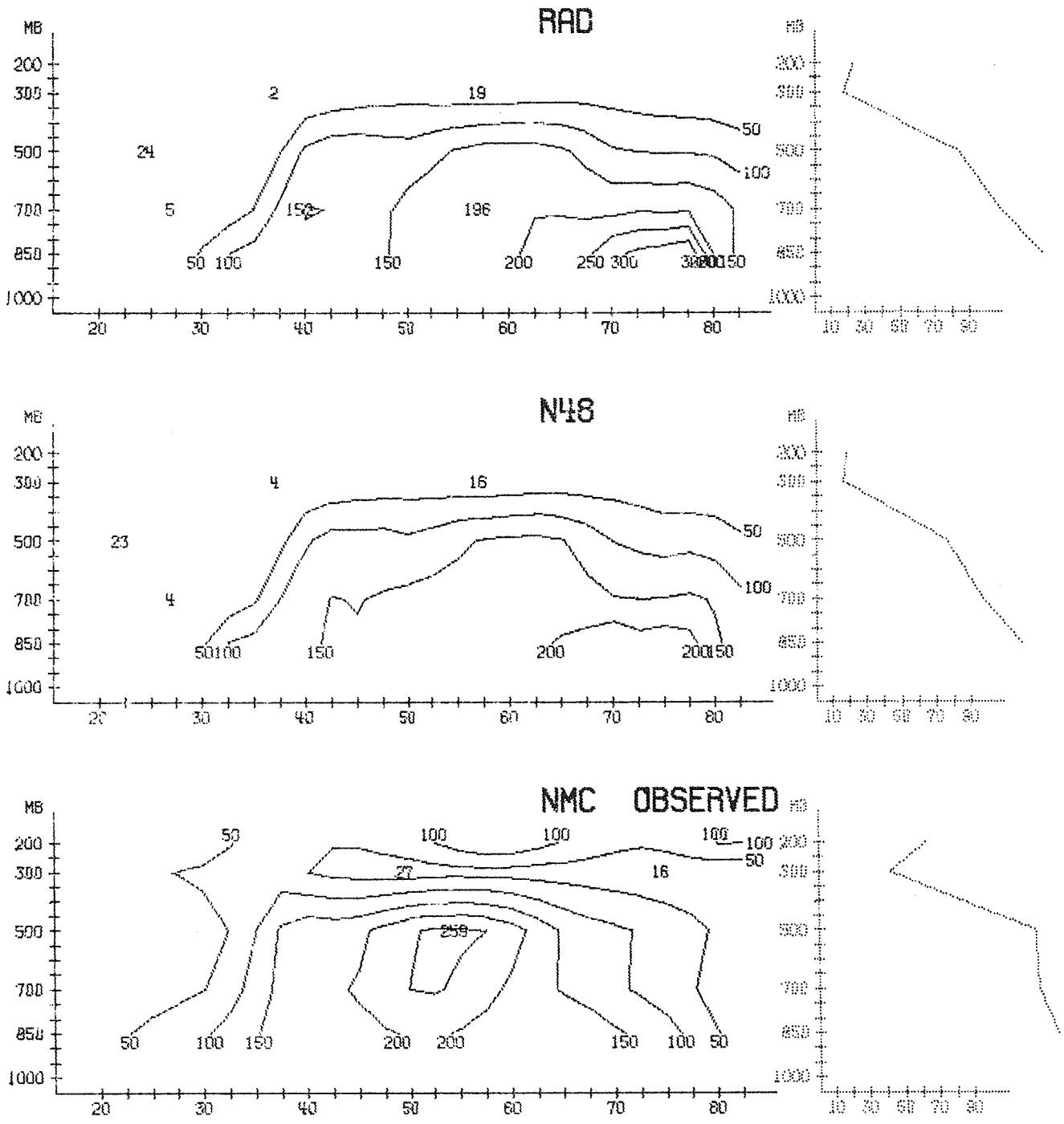

Fig. 3.5.7 Latitude height cross-section of available potential energy averaged over days $4\frac{1}{2}$ to 7 for both runs and for the observations.

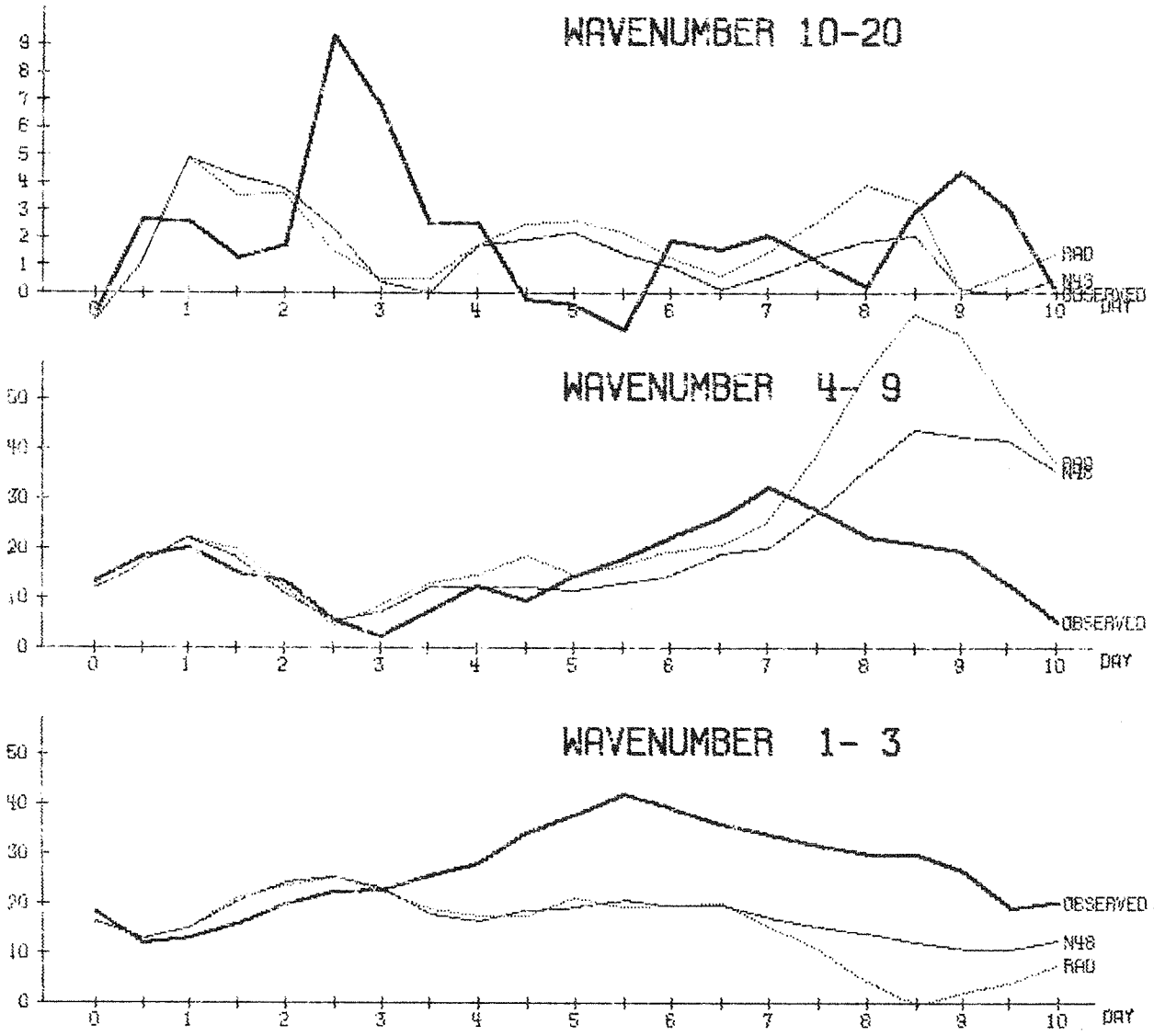

Fig. 3.5.8 Time evolution of the conversion rate from zonal to eddy available potential energy for both runs and for the observations, averaged over the troposphere (200 - 1000 mb) for the region north of 20N.

EUROPEAN CENTRE FOR MEDIUM RANGE WEATHER FORECASTS

Research Department (RD)

Internal Report No. 20

No. 1 Users Guide for the GFDL Model (November 1976)

No. 2 The effect of Replacing Southern Hemispheric Analyses by Climatology on Medium Range Weather Forecasts (January 1977)

No. 3 Test of a Lateral Boundary Relaxation Scheme in a Barotropic Model (February 1977)

No. 4 Parameterization of the Surface Fluxes (February 1977)

No. 5 An Improved Algorithm for the Direct Solution of Poisson's Equation over Irregular Regions (February 1977)

No. 6 Comparative Extended Range Numerical Integrations with the ECMWF Global Forecasting Model 1 : The N24, Non-Adiabatic Experiment (March 1977)

No. 7 The ECMWF Limited Area Model (March 1977)

No. 8 A Comprehensive Radiation Scheme designed for Fast Computation (May 1977)

No. 9 Documentation for the ECMWF Grid-Point Model (May 1977)

No. 10 Numerical Tests of Parameterization Schemes at an Actual Case of Transformation of Arctic Air (June 1977)

No. 11 Analysis Error Calculations for the FGGE (June 1977)

No. 12 Normal Modes of a Barotropic Version of the ECMWF Grid-Point Model (July 1977)

No. 13 Direct Methods for the Solution of the Discrete Poisson Equation : Some Comparisons (July 1977)

No. 14 On the FACR (ℓ) Algorithm for the Discrete Poisson Equation (September 1977)

No. 15 A Routine for Normal Mode Initialization with Non-Linear Correction for a Multi-Level Spectral Model with Triangular Truncation (August 1977)

No. 16 A Channel Version of the ECMWF Grid-Point Model (December 1977)

No. 17 A Comparative Study of Some Low Resolution Explicit and Semi-Implicit Spectral Integrations (August 1978)

EUROPEAN CENTRE FOR MEDIUM RANGE WEATHER FORECASTS
Research Department (RD)
Internal Report No. 20

No. 18 Verification and storing with empirical orthogonal functions

No. 19 Documentation of the ECMWF Spectral Model

No. 20 A study of the effect of an interactive radiation scheme on a medium range forecast